Journal of *Marine Science and Engineering*

MDPI

Article

Underwater Acoustic Integrated Sensing and Communication: A Spatio-Temporal Freshness for Intelligent Resource Prioritization

Ananya Hazarika and Mehdi Rahmati *

Electrical and Computer Engineering Department, Cleveland State University, Cleveland, OH 44115, USA; a.hazarika@vikes.csuohio.edu

* Correspondence: m.rahmati@csuohio.edu

Abstract

Underwater acoustic communication faces significant challenges including limited bandwidth, high propagation delays, severe multipath fading, and stringent energy constraints. While integrated sensing and communication (ISAC) has shown promise in radio frequency systems, its adaptation to underwater environments remains challenging due to the unique acoustic channel characteristics and the inadequacy of traditional delay-based performance metrics that fail to capture the spatio-temporal value of information in dynamic underwater scenarios. This paper presents a comprehensive underwater ISAC framework centered on a novel Spatio-Temporal Information-Theoretic Freshness metric that fundamentally transforms resource allocation from delay minimization to value maximization. Unlike conventional approaches that treat all data equally, our spatio-temporal framework enables intelligent prioritization by recognizing that obstacle detection data directly ahead of an autonomous underwater vehicle (AUV) require immediate processing. Our framework addresses key underwater ISAC challenges through spatio-temporal-guided power allocation, adaptive beamforming, waveform optimization, and cooperative sensing strategies. Multi-agent reinforcement learning algorithms enable coordinated resource allocation and mission-critical information prioritization across heterogeneous networks comprising surface buoys, AUVs, and static sensors. Extensive simulations in realistic Munk profile acoustic environments demonstrate significant performance improvements. The spatio-temporal framework successfully filters spatially irrelevant data, resulting in substantial energy savings for battery-constrained underwater nodes.

Keywords: integrated sensing and communications; intelligence; underwater acoustic communications; sonar

check for updates

Academic Editor: Weicheng Cui

Received: 21 July 2025
Revised: 26 August 2025
Accepted: 1 September 2025
Published: 10 September 2025

Citation: Hazarika, A.; Rahmati, M. Underwater Acoustic Integrated Sensing and Communication: A Spatio-Temporal Freshness for Intelligent Resource Prioritization. *J. Mar. Sci. Eng.* **2025**, *13*, 1747. https://doi.org/10.3390/jmse13091747

Copyright: © 2025 by the authors. Licensee MDPI, Basel, Switzerland. This article is an open access article distributed under the terms and conditions of the Creative Commons Attribution (CC BY) license (https://creativecommons.org/licenses/by/4.0/).

1. Introduction

Underwater acoustic communications and networks are crucial for collecting oceanographic data, monitoring the environment, conducting underwater exploration, surveillance, and security, and disaster prevention [1]. However, they operate under conditions of extreme scarcity, such as very low bandwidth, large delay, harsh multipath, and tight energy budgets. In such settings, the central challenge is not only delivering data quickly, but deciding which data are worth spending energy and time on. The system must facilitate communication and localization among heterogeneous static sensors, autonomous underwater vehicles (AUVs), remotely operated vehicles (ROVs), and surface stations/buoys

in the challenging aquatic environment, all of which significantly influence system design, communication protocols, and sensing strategies. However, the underwater acoustic channel imposes significant inherent constraints, including bandwidth limitations, substantial propagation delays, severe multipath interference causing intersymbol interference, Doppler shifts, frequency-dependent attenuation, and stringent energy constraints for battery-powered nodes [2]. Reverberation in active sensing, which creates clutter echoes, and ambient and mostly non-Gaussian noise in passive sensing are central challenges in underwater acoustic sensing. The presence of diverse entities, i.e., heterogeneous static and dynamic nodes, further highlights these challenges and underscores the need for more efficient and versatile solutions. The sound profile is highly environment-dependent and varies with factors such as depth, salinity, water temperature, seabed composition, and biological activity, all of which further complicate the design of underwater acoustic systems.

Conventional underwater systems treat communication and sensing as separate entities due to their primary objectives, their fundamental performance metrics, and system designs. Communication emphasizes data transfer reliability, delay control, and throughput efficiency, while sensing focuses on extracting environmental or target detection and estimation, such as location, motion, or structure, through passive or active acoustic measurements. A waveform designed for high-resolution sensing may not be suitable for communications due to its low data rate and high susceptibility to inter-symbol interference (ISI) from multipath. On the other hand, a waveform designed for high-data-rate communications may provide poor performance for sensing and ranging due to a low-resolution ambiguity function. Operating these systems independently may result in duplicated hardware, inefficient spectrum utilization, unnecessary energy overhead, and increased deployment complexity. These constraints restrict traditional systems to either high data rates at short ranges or very low rates at long ranges, limiting their ability to support mission-critical applications such as AUV navigation, environmental monitoring, and multi-vehicle coordination. To overcome these shortcomings, integrated sensing and communication (ISAC) has emerged as a transformative paradigm in radio frequency spectrum. ISAC enables sensing and communication to share the same waveform, spectrum, and hardware resources, thereby theoretically optimizing spectrum utilization and improving overall efficiency. In the underwater acoustics context, deploying ISAC can be a challenge. It can be a suboptimal solution for both functions, potentially operating through complementary modes tailored to the characteristics of the acoustic channel, i.e., (i) *coexistence mode*, where sensing and communication share the acoustic spectrum via time or code division multiplexing; (ii) *joint waveform design*, which creates signals optimized for both functions, exploiting channel impairments such as multipath and Doppler effects as valuable sensing information; and (iii) *integrated hardware architectures*, utilizing shared transducer arrays for transmitting communication signals and receiving sensing echoes, significantly reducing system complexity [3]. The information-sharing mechanisms leverage sensing data to improve communication performance through enhanced channel estimation, while communication signals contribute to sensing by interacting with the environment. This dual functionality provides inherent localization and tracking capabilities, which are critical for AUV navigation and control within coordinated multi-vehicle operations. In addition, it improves the robustness of communication by adapting to dynamic and variable underwater acoustic channel conditions. However, while ISAC introduces clear advantages in terms of efficiency and functionality, it inherently involves trade-offs. Furthermore, existing implementations remain constrained by their dependence on traditional performance measurement metrics.

Despite these advancements, a critical limitation of current underwater networks is their reliance on traditional performance measurement metrics, such as end-to-end de-

lay, which fail to capture the spatio-temporal value of information in harsh and dynamic underwater environments. End-to-end delay metrics, such as round-trip times for sonar pulses or packet transmission delays, quantify temporal latency but overlook the directional relevance and freshness of data relative to mission objectives. For example, sonar systems measure delays to estimate target ranges but do not account for whether detected objects are mission-critical, such as obstacles in an AUV's heading, or less relevant, such as stable seabed features. Similarly, communication systems prioritize minimizing packet delivery delays without considering the spatial context of the data, such as its relevance to tasks including obstacle avoidance or environmental monitoring. This approach becomes particularly inadequate when prior knowledge, such as environmental maps or known node positions, is available or estimated, as delay-based metrics cannot deprioritize redundant data, leading to inefficient utilization of bandwidth and energy, which are critical resources in battery-constrained underwater networks [4]. The inability to account for the spatial and temporal relevance of information highlights the need for a novel metric that integrates both dimensions to effectively prioritize mission-critical data. Underwater ISAC systems involve diverse platforms such as AUVs, ROVs, and fixed buoys, each serving distinct operational roles. In this work, we emphasize AUV-aided ISAC as the primary motivating scenario, while other platforms are considered only as complementary elements. Table 1 outlines the major technical and operational challenges in underwater acoustic networks, ranging from fundamental physical-layer limitations to the system-level deployment issues of ISAC. Addressing these challenges motivates the introduction of the proposed spatio-temporal metric, which shifts the focus from conventional delay-based metrics to value-oriented prioritization of information.

Table 1. Key challenges in implementing ISAC for underwater acoustic networks.

Challenge	Description
Standardization	Lack of standardized protocols and regulations for ISAC in underwater, hindering interoperability and widespread adoption.
Interoperability	Ensuring seamless cooperation between different systems is challenging due to diverse hardware and vendors.
Technology Maturity	ISAC application to underwater acoustics remains in early stages, lacking mature technologies or commercial products.
Security	Integration of sensing and communication introduces vulnerabilities, including eavesdropping on sensing data and potential sensing-based attacks.
Robustness	Dynamic underwater sound profiles due to the variability of temperature, salinity, and pressure significantly impact both sensing and communication performance.
Energy Efficiency	Power consumption is critical for battery-powered nodes, necessitating designs that minimize energy usage while maximizing performance. Active sensing requires a high power, while communications uses an average-to-low power normally.
Waveform Design	Designing a waveform that serves as both a high-resolution sensing and a high-data-rate communications waveform is a challenge.
Processing Complexity	Real-time joint processing is computationally intensive, presenting a common challenge in ISAC.

This paper presents a comprehensive underwater acoustic ISAC framework that introduces a novel Spatio-Temporal Information-Theoretic Freshness (STIF) metric to address the fundamental challenges of underwater acoustic networks. The proposed framework optimizes resource allocation across the physical, waveform, processing, and network

layers, unlocking the transformative potential of integrated sensing and communication in energy- and bandwidth-constrained underwater environments. The main contributions are threefold, as given below.

1. We introduce the STIF metric, which integrates temporal freshness, spatial relevance, reliability, and predictive components to quantify the value of information. Unlike conventional delay- or Age of Information (AoI)-based metrics, STIF enables intelligent prioritization of mission-critical data in dynamic underwater networks.
2. We develop a complete UW-ISAC framework that leverages STIF for cross-layer optimization, enabling energy-efficient and scalable resource allocation. The framework shifts the focus from delay minimization to value maximization, improving both coverage and robustness in realistic acoustic environments.
3. We emphasize AUV-aided ISAC as the primary motivating use case and validate the proposed framework through extensive simulations under realistic Munk profile conditions. The results demonstrate that STIF significantly outperforms conventional AoI- and delay-based approaches in terms of efficiency, robustness, and mission-oriented performance.

By integrating spatial freshness with temporal freshness, the STIF metric enables the intelligent prioritization of data, focusing limited bandwidth and energy resources on information critical for operational objectives, such as AUV navigation or environmental monitoring. The metric's ability to leverage prior knowledge, such as mapped obstacles or established communication links, enables it to prioritize non-redundant updates, allocating resources to dynamic or uncertain regions.

The rest of the paper is organized as follows. Section 2 reviews the current state-of-the-art in underwater acoustic communications, sensing systems, and emerging ISAC approaches, positioning our work within the broader research landscape. Section 3 presents the comprehensive system model, including the heterogeneous node architecture, underwater acoustic channel characterization, and time-varying connectivity graph formulation. Section 4 details the signal processing framework for underwater acoustic ISAC, covering active and passive sensing models, communication schemes using Orthogonal Frequency Division Multiplexing (OFDM), and the innovative composite signal design that enables simultaneous sensing and communication through time-frequency orthogonality. Section 5 introduces the novel Spatio-Temporal Information-Theoretic Freshness (STIF) metric, providing rigorous mathematical formulations for its four key components and demonstrating how it captures the spatio-temporal value of information in an underwater environment. Section 6 presents the STIF-guided resource allocation strategies, including power allocation, adaptive beamforming, waveform optimization, and cooperative sensing mechanisms enabled by multi-agent reinforcement learning. Section 7 provides comprehensive simulation results using realistic sound profiles, validating the framework's performance across diverse operational scenarios and demonstrating significant improvements in energy efficiency, sensing quality, and communication throughput. Finally, Section 8 concludes the paper with a summary of key contributions and outlines promising directions for future research in underwater ISAC systems.

2. Related Works

The field of underwater acoustic communications and networks has undergone significant evolution over the past two decades, driven by the need for reliable communication and environmental sensing in challenging underwater environments. Early research focused on addressing the inherent limitations of underwater acoustic channels, such as limited bandwidth, high propagation delays, frequency-dependent attenuation, and severe multipath fading. Sozer et al. [2] provided foundational insights into underwater acoustic

communications, highlighting the trade-offs between data rates and range. Subsequent surveys, such as [5,6], have explored underwater wireless sensor networks with a focus on energy efficiency and routing protocols for applications including oceanographic data collection and environmental monitoring. Authors in [7,8] further discussed high-data-rate short-range links versus low-data-rate long-range communications, where the work in [8] proposed an acoustic Reconfigurable Intelligent Surface (RIS) system using piezoelectric reflector arrays to enable wideband beamforming and motion-resilient high-data-rate long-range underwater communication without requiring hardware changes at end devices. Underwater sensing has traditionally been treated separately from communication, with passive and active sonar systems. Active sonars use pulses for echo ranging, while passive sonars employ signal processing techniques to extract information from received signals in the presence of ambient noise [9]. Li et al. [10] reviewed advances in underwater acoustic sensor networks, focusing on localization and target tracking. Hague et al. [11] introduced a Generalized Sinusoidal Frequency Modulation (GSFM) pulse for active sonars, which preserves Doppler sensitivity while reducing range sidelobes, achieving a desirable ambiguity function. Wang et al. [12] proposed multidimensional evaluation methods for sonar detection efficiency based on spatio-temporal interactions, which aligns with the need for geometry-aware metrics but lacks integration with communication systems. ISAC has garnered substantial attention in radio frequency for 6G networks, enabling spectrum sharing between radar and communication [3]. The authors in [13] surveyed ISAC for smart oceans, covering integrated sensing, communication, and computing networks, discussing the potential for underwater deployments. Similarly, the surveyed integration of localization, communication, and control in underwater acoustic sensor networks has been discussed in [3], providing insights into cooperative designs that our framework extends with STIF prioritization. Freshness metrics, such as AoI, have been applied to underwater networks for delay-sensitive applications [14]. The work in [12] emphasized the need for multidimensional evaluation methods that account for dynamic spatio-temporal interactions in sonar detection efficiency. Cognitive approaches in [4] discussed resource allocation in underwater cognitive acoustic networks but overlooked spatio-temporal freshness. Early surveys on underwater sensor network challenges and protocols have been introduced in [15] that emphasize the need for adaptive metrics. Recent AI-driven advancements in underwater acoustic sensor networks have led to the development of intelligent routing protocols that leverage machine learning and adaptive decision-making to enhance reliability, scalability, and energy efficiency, as detailed in [16]. Complementing these efforts, the authors in [17] explored the role of Software-Defined Networking (SDN) and virtualization technologies in underwater acoustic networks, highlighting how centralized control and programmability can address dynamic underwater conditions and improve network management. The growing interest in deploying cost-effective solutions for large-scale ocean monitoring has also led to research on low-cost sensor networks, with the discussion in [18] surveying recent innovations in energy-aware sensing, hardware miniaturization, and modular deployment. Despite recent advancements, there are still notable gaps in the seamless integration of sensing and communication with spatio-temporal awareness and prioritization. To tackle this issue, our work presents a new framework that quantifies the relevance of information based on its spatial location and temporal freshness. This approach, referred to as STIF, facilitates informed decision-making and efficient resource allocation.

3. System Model

The underwater acoustic ISAC framework operates within a heterogeneous underwater network comprising surface buoys, AUVs, ROVs, and static sensor nodes, deployed in a three-dimensional region $\Omega \subset \mathbb{R}^3$. This section defines the network framework

(Figure 1), acoustic channel models, waveform design for data transmission and reception, and the optimization problem, providing the foundation for ISAC in an underwater environment constrained by limited bandwidth, propagation delays, severe multipath interference, Doppler shifts, and energy limitations [2,5]. The network consists of a set of nodes $\mathcal{N} = \{1, \ldots, N\}$, where each node, indexed by $i \in \mathcal{N}$, is characterized by its position $\mathbf{r}_i(t) = [x_i(t), y_i(t), z_i(t)]^T \in \Omega$, velocity $\mathbf{v}_i(t)$ (zero for static nodes), and operational mode $m_i(t) \in \{\text{sensing}, \text{communication}, \text{dual}\}$. Surface buoys, synchronized via GPS for precise timing, act as network coordinators, employing hydrophone sub-arrays in linear or circular configurations for omnidirectional sensing and long-range communication. AUVs/ROVs, with mobility for agile navigation, use hydrophone sub-arrays in circular or volumetric configurations for high-resolution sensing, such as obstacle detection. Static sensor nodes, fixed or tethered, utilize hydrophone sub-arrays in linear configurations for energy-efficient environmental monitoring. Tonpilz projectors transmit composite waveforms, while hydrophone sub-arrays receive signals and echoes [10]. The network forms a time-varying connectivity graph $\mathcal{G}(t) = (\mathcal{N}, \mathcal{E}(t))$, where the edge set $\mathcal{E}(t) = \{(i, j) : \text{SNR}_{ij}(t) \geq \gamma_{\text{th}}\}$ defines communication links based on the signal-to-noise ratio (SNR), determined by transmitted power, channel attenuation, and ambient noise.

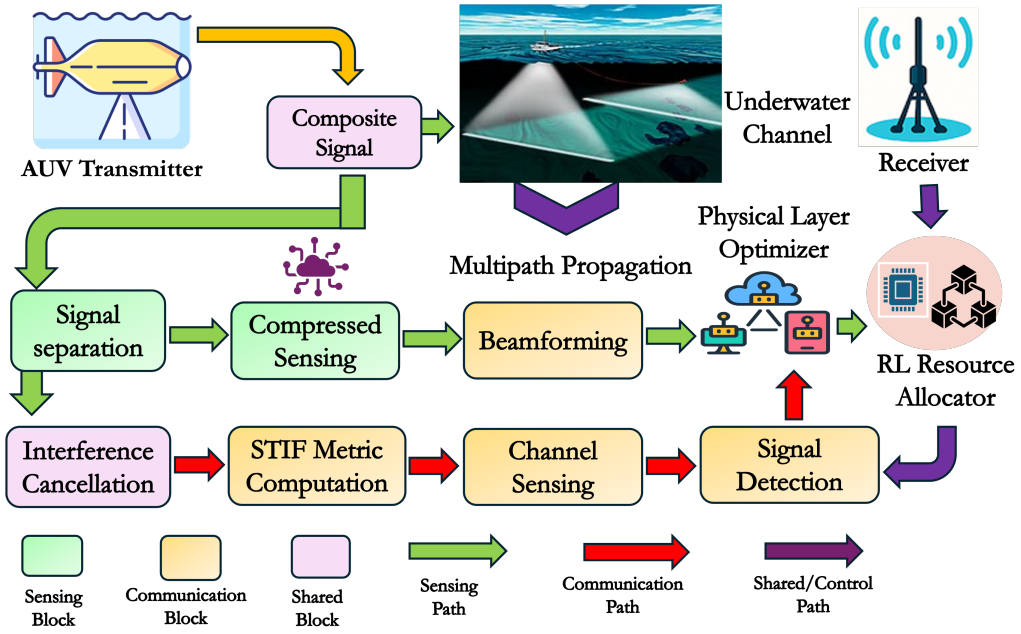

Figure 1. Block diagram of the proposed UW-ISAC framework, showing the joint sensing-and-communication signal chain alongside STIF-driven optimization and feedback resource allocation through the underwater acoustic channel.

The acoustic channel between nodes i and j is modeled as a time-varying, multipath channel with a limited number of dominant propagation paths, resulting from direct transmission and reflections from the ocean surface, bottom, and thermoclines. The channel impulse response is

$$h_{ij}(t, \tau) = \sum_{l=1}^{L_{ij}(t)} A_{l,ij}(t) \delta(\tau - \tau_{l,ij}(t)) \tag{1}$$

where $L_{ij}(t)$ captures the direct path and dominant reflections. The propagation delay of path l is $\tau_{l,ij}(t) = d_{l,ij}(t)/c(t)$, with $d_{l,ij}(t)$ as the path distance and $c(t)$ as the sound speed, modeled by the Chen–Millero polynomial accounting for temperature and depth variations [2]. The complex amplitude $A_{l,ij}(t)$ of each path integrates geometric spreading; frequency-dependent absorption, calculated via Thorp's empirical formula and small-scale

fading; and $\xi_{l,ij}(t) \sim \mathcal{CN}(0,1)$ modeling Rayleigh fading induced by water currents and surface waves.

4. Signal Processing for UW ISAC

In this section, we propose a unified signal processing framework for underwater ISAC as shown in Figure 1 that jointly supports communication and sensing within the same environment. The framework is designed to efficiently exploit the shared spectrum and hardware resources, mitigate underwater channel impairments such as multipath and Doppler spread, and adapt signal structures to mission-driven objectives.

4.1. Sensing Model

The sensing model in the UW framework is designed to extract environmental and target information, such as range, velocity, and direction, using both active and passive acoustic techniques. Active sensing uses dedicated high-resolution pulses to probe the environment, while passive sensing leverages ambient sounds and communication signals from other nodes, enhancing energy efficiency and situational awareness. The model addresses the underwater channel's unique characteristics, including curved sound trajectories due to depth-dependent sound speed profiles, severe multipath effects, and Doppler shifts induced by ocean currents and platform motion [2].

4.1.1. Active Sensing with Short-Pulse Sonar

Active sensing employs short-duration acoustic pulses, specifically, Gaussian-enveloped Sinusoidal Frequency-Modulated (GSFM) signals [19], to achieve high temporal resolution for ranging and target detection. The sensing waveform that provide optimal time-frequency localization $x_i^{(\text{sens})}(t)$ for node i is defined as

$$x_i^{(\text{sens})}(t) = A_s \exp\left(-\frac{t^2}{2\sigma^2}\right) \cos\left(2\pi f_c t + \pi k_r t^2\right), \tag{2}$$

where A_s is the amplitude, σ controls the pulse duration, f_c is the carrier frequency, and k_r is the chirp rate for frequency modulation, enhancing Doppler resolution. The Gaussian envelope ensures smooth spectral characteristics, reducing out-of-band emissions that could interfere with communication channels. The chirp modulation [20] enhances Doppler resolution through the ambiguity function properties, enabling simultaneous range and velocity estimation. The range resolution achieved by this waveform is $\Delta R = \frac{c}{2B_{\text{eff}}}$ where $B_{\text{eff}} = \sqrt{1/\sigma^2 + (k_r T_p)^2}$ is the effective bandwidth and T_p is the pulse duration. This formulation ensures high-resolution ranging (e.g., $\Delta R \approx 0.75\,\text{m}$ for $B_{\text{eff}} = 1\,\text{kHz}$ for typical speed of sound) suitable for detecting closely spaced targets in cluttered underwater environments.

The received echo from targets and environmental features, after propagation through the multipath channel, is represented by

$$y_j^{(\text{sens})}(t) = \sum_{l=1}^{L_{ij}(t)} A_{l,ij}(t)\mathbf{a}_j^H(\theta_{l,ij})\mathbf{w}_i(t)x_i^{(\text{sens})}\left(t - \tau_{l,ij}(t)\right)e^{j2\pi\nu_{l,ij}(t)t} + n_j(t) \tag{3}$$

where each path l is characterized by complex amplitude $A_{l,ij}(t)$, propagation delay $\tau_{l,ij}(t)$, and Doppler shift $\nu_{l,ij}(t)$. The array response $\mathbf{a}_j(\theta_{l,ij})$ captures the spatial signature, enabling direction-of-arrival estimation, and $\mathbf{w}_i(t)$ is the transmit beamforming/precoding vector at

node i, used to steer the sensing signal toward the intended direction. Signal processing for active sensing employs matched filtering followed by adaptive algorithms, given by

$$z_j(t) = \int y_j^{(\text{sens})}(\tau) x_i^{(\text{sens})*}(\tau - t) d\tau, \tag{4}$$

where $z_j(t)$ peaks at delays corresponding to target ranges. The matched filter output $z_j(t)$ exhibits peaks at delays corresponding to target ranges. To resolve closely spaced targets and mitigate multipath interference, we apply compressed sensing techniques that exploit the sparsity of the target scene, represented as

$$\hat{\boldsymbol{\eta}} = \arg\min_{\boldsymbol{\eta}} \|\mathbf{z} - \boldsymbol{\Phi}\boldsymbol{\eta}\|_2^2 + \lambda \|\boldsymbol{\eta}\|_1 \tag{5}$$

where $\boldsymbol{\Phi}$ is a dictionary of delayed and Doppler-shifted pulse replicas, and λ controls the sparsity level.

4.1.2. Passive Sensing

Passive sensing complements active sensing by extracting information from ambient environmental sounds (e.g., biologics, currents, surface waves) and communication signals from other nodes, without dedicated sensing pulses, making it energy-efficient for battery-powered nodes. The received signal for passive sensing is

$$y_j^{(\text{passive})}(t) = \sum_{k \in \mathcal{N}} \sum_{l=1}^{L_{kj}(t)} A_{l,kj}(t) \mathbf{a}_j^H(\theta_{l,kj}) x_k^{(\text{comm})}\Big(t - \tau_{l,kj}(t)\Big) e^{j2\pi\nu_{l,kj}(t)t} + n_j^{(\text{env})}(t), \tag{6}$$

where $x_k^{(\text{comm})}(t)$ is the communication signal from node k, and $n_j^{(\text{env})}(t)$ includes ambient environmental noise. Spectral analysis and beamforming estimate environmental features (e.g., current-induced Doppler shifts) or localize nodes via direction-of-arrival estimation. Spectral analysis and beamforming are applied to estimate environmental features (e.g., current-induced Doppler shifts) and localize nodes via direction-of-arrival estimation, improving situational awareness in dynamic underwater settings.

4.2. Communication Model

Orthogonal Frequency Division Multiplexing (OFDM) is employed as the primary modulation scheme due to its robustness against multipath fading and ability to support high data rates in wideband channels [2]. The communication waveform $x_i^{(\text{comm})}(t)$ for node i is an OFDM signal with N_c subcarriers modulated with data symbols as

$$x_i^{(\text{comm})}(t) = \sum_{k=0}^{N_c-1} d_k(t) e^{j2\pi(f_c + k\Delta f)t}, \quad 0 \le t \le T_s, \tag{7}$$

where $d_k(t)$ is the data symbol on the k-th subcarrier, f_c is the carrier frequency, $\Delta f = \frac{B}{N_c}$ is the subcarrier spacing, and $T_s = \frac{1}{\Delta f}$ is the OFDM symbol duration. A cyclic prefix of duration $T_{\text{CP}} \ge \tau_{\max}$ precedes each OFDM symbol, where $\tau_{\max}$ is the maximum multipath delay spread. This guard interval eliminates inter-symbol interference and enables simple frequency-domain equalization. After propagation through the multipath channel, the received communication signal at node j becomes

$$y_j^{(\text{comm})}(t) = \sum_{l=1}^{L_{ij}(t)} A_{l,ij}(t) \mathbf{a}_j^H(\theta_{l,ij}) \mathbf{w}_i(t) x_i^{(\text{comm})}\Big(t - \tau_{l,ij}(t)\Big) e^{j2\pi\nu_{l,ij}(t)t} + n_j(t). \tag{8}$$

After CP removal and FFT processing, the received signal on the k-th subcarrier becomes

$$Y_{j,k} = H_{ij,k} d_k + N_{j,k}, \tag{9}$$

where $H_{ij,k}$ is the channel frequency response, and $N_{j,k}$ is the noise component.

4.3. ISAC Signal Model

We propose an innovative signal processing algorithm (See Algorithm 1) that enables simultaneous sensing and communication for the UW-ISAC framework by extracting environmental information (range, velocity, and direction) and transmitting data reliably in the challenging underwater acoustic environment. The proposed ISAC signal model integrates GSFM pulses for high-resolution sensing and OFDM for robust communication, utilizing time-frequency orthogonality to minimize interference. This approach optimizes spectrum and energy efficiency for battery-powered nodes, addressing key challenges such as energy constraints, robustness to environmental variations, and interoperability (Table 1). The composite transmitted signal $x_i(t)$ from node i combines sensing and communication components and is represented as

$$x_i(t) = \rho_i(t)\, x_i^{(\text{sens})}(t) + \big(1 - \rho_i(t)\big)\, x_i^{(\text{comm})}(t), \tag{10}$$

where $x_i^{(\text{sens})}(t)$ is the GSFM sensing waveform (Equation (2)), $x_i^{(\text{comm})}(t)$ is the OFDM communication waveform (Equation (7)), and $\rho_i(t) \in [0, 1]$ is the power allocation factor balancing sensing and communication objectives. The sensing and communication components are allocated to distinct time slots or frequency sub-bands to ensure orthogonality and minimize interference.

Signal Separation: The received signal $y_j(t)$ is separated into sensing $y_j^{(\text{sens})}(t)$ and communication $y_j^{(\text{comm})}(t)$ components using time-frequency orthogonality to minimize interference. Short GSFM pulses (duration 0.1–1 ms) are transmitted in guard intervals, while OFDM signals occupy data slots (duration $T_s = 10\,\text{ms}$). Time-domain separation uses rectangular windowing as shown below:

$$y_j^{(\text{sens})}(t) = y_j(t)\text{rect}\left(\frac{t - t_s}{T_{\text{pulse}}}\right), \quad y_j^{(\text{comm})}(t) = y_j(t)\text{rect}\left(\frac{t - t_c}{T_s}\right), \tag{11}$$

where $\text{rect}(\cdot)$ is the rectangular window function, and t_s, t_c are the start times of sensing and communication slots, respectively. Alternatively, if the system is designed to allow frequency-domain separation, a dedicated sub-band can be allocated to sensing, while the remaining frequency band is used for communication, expressed as follows:

$$y_j^{(\text{sens})}(t) = \mathcal{F}^{-1}\{\mathcal{F}\{y_j(t)\} H_{\text{sens}}(f)\}, \quad y_j^{(\text{comm})}(t) = \mathcal{F}^{-1}\{\mathcal{F}\{y_j(t)\} H_{\text{comm}}(f)\}, \tag{12}$$

where $\mathcal{F}$ and $\mathcal{F}^{-1}$ denote the Fourier transform and its inverse, and $H_{\text{sens}}(f)$, $H_{\text{comm}}(f)$ are bandpass filters for the respective bands. The received signal at node j, after propagation through the multipath channel, is

$$y_j(t) = \sum_{l=1}^{L_{ij}(t)} A_{l,ij}(t)\, \mathbf{a}_j^H(\theta_{l,ij})\, \mathbf{w}_i(t)\, x_i(t - \tau_{l,ij}(t))\, e^{j2\pi\nu_{l,ij}(t)t} + n_j(t), \tag{13}$$

where $A_{l,ij}(t)$, $\tau_{l,ij}(t)$, $\nu_{l,ij}(t)$, and $\mathbf{a}_j(\theta_{l,ij})$ are the channel amplitude, delay, Doppler shift, and array response for path l, respectively, and $n_j(t)$ is Gaussian noise.

Doppler Compensation: Doppler shifts, caused by relative node velocities, are estimated via FFT analysis and applied to compensate both streams as shown below:

$$\tilde{y}_j^{(\text{sens})}(t) = y_j^{(\text{sens})}(t)e^{-j2\pi\hat{v}_{l,ij}t}, \quad \tilde{y}_j^{(\text{comm})}(t) = y_j^{(\text{comm})}(t)e^{-j2\pi\hat{v}_{l,ij}t}. \tag{14}$$

Sensing Processing: For active sensing, matched filtering is applied to $\tilde{y}_j^{(\text{sens})}(t)$ to estimate target ranges and directions as given by $z_j(t)$ where $z_j(t)$ peaks at delays corresponding to ranges $R_{l,ij} = \frac{c\tau_{l,ij}}{2}$. Compressed sensing resolves multipath components by $\hat{\boldsymbol{\eta}}$. For passive sensing, beamforming estimates directions of arrival from $\tilde{y}_j^{(\text{passive})}(t)$ as shown below:

$$\hat{\theta}_{kj} = \arg\max_{\theta} \left| \mathbf{w}_j^H \mathbf{a}_j(\theta) \tilde{y}_j^{(\text{passive})}(t) \right|^2. \tag{15}$$

The sensing quality is then quantified as

$$Q_{\text{sens}} = \sum_{l=1}^{L_{ij}(t)} \left(1 - \frac{|\hat{R}_{l,ij} - R_{l,ij}|}{R_{\max}} - \frac{|\hat{v}_{l,ij} - v_{l,ij}|}{v_{\max}} \right). \tag{16}$$

Communication Processing: The communication stream $\tilde{y}_j^{(\text{comm})}(t)$ is then processed by first removing the cyclic prefix, then applying FFT, and performing minimum mean square error (MMSE) equalization, represented by

$$\hat{d}_k = \frac{H_{ij,k}^* Y_{j,k}}{|H_{ij,k}|^2 + \frac{N_0}{P_i}}, \tag{17}$$

where $H_{ij,k}$ is the channel frequency response (Equation (9)), $Y_{j,k}$ is the received subcarrier signal, N_0 is noise power, and P_i is subcarrier power. The throughput is

$$R_{\text{comm}} = \sum_{k=0}^{N_c-1} \log_2 \left(1 + \frac{P_i |H_{ij,k}|^2}{N_0} \right). \tag{18}$$

Interference Cancellation: Successive interference cancellation (SIC) is performed to mitigate residual interference between sensing and communication streams and is shown by

$$\tilde{y}_j^{(\text{comm,SIC})}(t) = \tilde{y}_j^{(\text{comm})}(t) - \sum_{l=1}^{L_{ij}(t)} \hat{A}_{l,ij} \mathbf{a}_j^H(\hat{\theta}_{l,ij}) \mathbf{w}_i(t) x_i^{(\text{sens})}(t - \hat{\tau}_{l,ij}) e^{j2\pi\hat{v}_{l,ij}t}, \tag{19}$$

where $\hat{A}_{l,ij}$, $\hat{\tau}_{l,ij}$, and $\hat{\theta}_{l,ij}$ are estimated sensing parameters. The process iterates to refine both sensing and communication outputs.

Optimization: Power allocation $\rho_i(t)$, beamforming weights $\mathbf{w}_i(t)$, and subcarrier power need to be optimized to balance sensing and communication performance such that

$$\rho_i^*(t) = \arg\max_{\rho_i(t) \in [0,1]} \left[\omega_c \int_{-\pi}^{\pi} R_{\text{comm}}(\rho_i(t), \theta_{ij}) d\theta + \omega_s \int_{-\pi}^{\pi} Q_{\text{sens}}(\rho_i(t), \theta_{ij}) d\theta \right], \tag{20}$$

subject to power constraints $P_i \leq P_{\max}$, where ω_c and ω_s are application-dependent weights balancing communication throughput and sensing quality. The framework supports robust operation in dynamic underwater environments, setting the stage for advanced resource allocation strategies discussed in subsequent sections.

Algorithm 1 Integrated Sensing and Communication Processing (ISAC).

Input: Received signal $y_j(t)$, composite signal $x_i(t)$, channel parameters
Output: Sensing estimates ($\hat{R}_{l,ij}$, $\hat{v}_{l,ij}$, $\hat{\theta}_{l,ij}$), communication symbols $\hat{d}_k$
Separate $y_j(t)$ into $y_j^{(\text{sens})}(t)$ and $y_j^{(\text{comm})}(t)$ using Equation (11) or (12)
Estimate Doppler shifts via FFT and compensate through $y_j^{(\text{sens})}(t)$ and $y_j^{(\text{comm})}(t)$ (Equation (14))
Sensing Processing:
    Apply matched filtering to $\tilde{y}_j^{(\text{sens})}(t)$ (Equation (4))
    Resolve multipath using compressed sensing (Equation (5))
    For passive sensing, estimate directions via beamforming (Equation (15))
Communication Processing:
    Remove cyclic prefix, apply FFT, and perform MMSE equalization (Equation (17))
Interference Cancellation:
    Perform SIC to refine communication stream (Equation (19))
    Iterate until convergence of sensing and communication estimates
Optimize power allocation $\rho_i(t)$, beamforming weights $\mathbf{w}_i(t)$, and subcarrier power using Equation (20)
Return: Sensing estimates ($\hat{R}_{l,ij}$, $\hat{v}_{l,ij}$, $\hat{\theta}_{l,ij}$), communication symbols $\hat{d}_k$

5. Spatio-Temporal Information-Theoretic Freshness (STIF) Metric

Traditional underwater acoustic networks rely heavily on end-to-end delay metrics to evaluate communication performance, focusing on the time taken for a packet to traverse from source to destination. However, such metrics fail to capture the spatial and temporal heterogeneity inherent in underwater environments, where the value of information is highly context-dependent. In a cluttered environment, information about obstacles directly ahead of an AUV is critically time-sensitive and must be acted upon within seconds, whereas data from behind or from stable regions can tolerate delays of minutes without compromising mission safety. This observation motivates the concept of spatial freshness, which we define as the time-varying value of information as a function of its directional origin relative to the receiver's current operational context. Unlike end-to-end delay, which treats all packets equally regardless of their spatial relevance, spatial freshness recognizes that information value degrades not only with time but also with angular deviation from mission-critical directions. This section introduces the STIF metric, which quantifies the value of information by integrating temporal freshness, spatial relevance via mutual information, and channel reliability, thereby ensuring efficient resource allocation in the resource-constrained underwater environment characterized by limited bandwidth. Information about an obstacle directly ahead requires immediate processing to enable collision avoidance, while bathymetric data from behind the vehicle may tolerate significant delays without compromising safety. This spatial asymmetry in information value becomes even more pronounced when combined with temporal aging; for instance, fresh obstacle data from ahead are critically valuable, while aged data from the same direction rapidly lose relevance. Hence, the novelty of this work depends on the STIF metric, which quantifies information freshness by combining temporal, spatial, reliability, and predictive relevance. Unlike AoI or delay, STIF directly captures the mission-critical value of information, particularly for AUV-aided ISAC. We detail STIF below based on the ISAC foundations.

5.1. STIF Metric Definition

The STIF metric quantifies the value of information transmitted or received between nodes i and j in the time-varying connectivity graph $\mathcal{G}(t) = (\mathcal{N}, \mathcal{E}(t))$. It integrates temporal freshness, spatial information relevance, channel reliability, and predictive value

to prioritize data critical for mission objectives while addressing challenges such as energy efficiency, robustness, and interoperability (Table 1). The STIF metric is defined as

$$F(\theta_{ij}, t) = \prod_{k \in \{S,T,Q,P\}} (\mathcal{C}_k(t) + \epsilon)^{\alpha_k}, \quad \sum_{k \in \{S,T,Q,P\}} \alpha_k = 1, \tag{21}$$

where θ_{ij} is the direction of arrival (DOA) of the signal from node j to node i, each $\mathcal{C}_k(t)$ corresponds to one of the four components—spatial relevance $I(\theta_{ij}, t)$ (labeled S), temporal freshness $F_t(t)$ (labeled T), channel reliability $Q_{ij}(t)$ (labeled Q), and predictive value $P_{ij}(t, \Delta t)$ (labeled P)—ϵ ensures numerical stability, and $\alpha_k \geq 0$ are weights tuned to mission requirements. The metric is normalized to ensure $F(\theta_{ij}, t) \in [0, 1]$, achieved by scaling the output if necessary, making it suitable for resource allocation and signal processing. This geometric mean formulation, inspired by information theory and decision theory, balances the contributions of each component while maintaining dimension consistency and robustness to zero-valued components. It supports both monostatic and multistatic ISAC scenarios, enabling efficient prioritization of mission-critical data in underwater acoustic networks characterized by multipath propagation and Doppler shifts.

5.2. Temporal Freshness Component

The temporal freshness component $F_t(t)$ models the degradation of information value over time, reflecting the time-sensitive nature of underwater applications:

$$F_t(t) = \exp\left(-\frac{t - t_{\text{update}}}{\lambda_t}\right), \tag{22}$$

where t_{update} is the timestamp of the data's last update, λ_t is a mission-specific time scale (e.g., 1 s for obstacle avoidance, 10 s for navigation, 60 s for environmental monitoring), and t is the current time. The exponential decay ensures that recent data, such as real-time obstacle detection, are prioritized. For instance, in AUV navigation, data about an obstacle detected 1 s ago are critical, while data from 10 s ago may be obsolete due to the AUV's movement. The parameter λ_t is tunable to adapt to various mission requirements, ensuring flexibility across applications.

5.3. Spatial Information Relevance

The spatial information relevance component $I(\theta_{ij}, t)$ quantifies the importance of data based on their directional alignment with mission-critical objectives, such as the AUV's heading ($\theta_{\text{mission}}(t)$). It is defined using mutual information to measure the relevance of data arriving from direction θ_{ij} as

$$I(\theta_{ij}, t) = \exp\left(-\frac{|\theta_{ij} - \theta_{\text{mission}}(t)|^2}{2\sigma_s^2}\right) \max\left(1, \log\left(1 + \frac{P(\theta_{ij}|\theta_{\text{mission}}(t))}{P(\theta_{ij})}\right)\right), \tag{23}$$

where $|\theta_{ij} - \theta_{\text{mission}}(t)|$ is the angular deviation in Euclidean space, σ_s is the angular spread, $P(\theta_{ij}|\theta_{\text{mission}}(t))$ is the conditional probability of receiving relevant data from direction θ_{ij}, and $P(\theta_{ij}) = \frac{1}{2\pi}$ is the uniform prior over $[-\pi, \pi]$ [21]. The conditional probability is modeled as a Gaussian distribution, as shown below:

$$P(\theta_{ij}|\theta_{\text{mission}}(t)) = \frac{1}{\sqrt{2\pi\sigma_s^2}} \exp\left(-\frac{|\theta_{ij} - \theta_{\text{mission}}(t)|^2}{2\sigma_s^2}\right). \tag{24}$$

In practice, $P(\theta_{ij}|\theta_{\text{mission}}(t))$ is computed using beamforming-based DOA estimation, where θ_{ij} is estimated from the array response $\mathbf{a}_j(\theta_{ij})$, and $\theta_{\text{mission}}(t)$ is derived from the

AUV's navigation system or mission planner. The $\max(1, \cdot)$ term ensures the mutual information contribution remains non-negative, addressing numerical stability for small probabilities. This formulation prioritizes data aligned with $\theta_{\text{mission}}(t)$, such as obstacles in the AUV's path, reflecting the spatial asymmetry described in Section 5.

5.4. Channel Reliability Factor

The channel reliability factor $Q_{ij}(t)$ accounts for signal quality under the underwater acoustic channel's challenges, denoted by

$$Q_{ij}(t) = \frac{\text{SNR}_{ij}(t)}{\text{SNR}_{ij}(t) + \kappa} \exp\left(-\alpha_{\text{eff}} d_{ij} - \sigma^2_{h,ij}\right), \tag{25}$$

where $\text{SNR}_{ij}(t)$ is the signal-to-noise ratio (Section 3), $\kappa = 1$ is a normalization constant, α_{eff} is the effective attenuation coefficient from Thorp's formula [2], d_{ij} is the Euclidean distance between nodes, and $\sigma^2_{h,ij}$ is the normalized delay spread:

$$\sigma^2_{h,ij} = \frac{\sum_{l=1}^{L_{ij}(t)} |A_{l,ij}(t)|^2 (\tau_{l,ij}(t) - \bar{\tau}_{ij})^2}{\sum_{l=1}^{L_{ij}(t)} |A_{l,ij}(t)|^2}, \tag{26}$$

where $\tau_{l,ij}(t)$ and $\bar{\tau}_{ij}$ are the propagation delay and mean delay for path l (Equation (1)). The terms $\exp(-\alpha_{\text{eff}} d_{ij})$ and $\exp(-\sigma^2_{h,ij})$ penalize absorption losses and multipath dispersion, respectively, ensuring reliable links are prioritized.

5.5. Multipath Aggregation

To account for multipath propagation, the STIF metric aggregates contributions from all paths $l \in \{1, \ldots, L_{ij}(t)\}$ such that

$$F_{ij}(t) = \sum_{l=1}^{L_{ij}(t)} w_l F(\theta_{l,ij}, t), \tag{27}$$

where $F(\theta_{l,ij}, t)$ is the STIF metric for path l (Equation (21)), and w_l is the weight proportional to path energy, given by

$$w_l = \frac{|A_{l,ij}(t)|^2}{\sum_{k=1}^{L_{ij}(t)} |A_{k,ij}(t)|^2}, \tag{28}$$

with $\theta_{l,ij}$ as the DOA for path l, estimated via beamforming. This ensures stronger paths contribute more to the overall freshness, while directional diversity is captured by $I(\theta_{l,ij}, t)$.

5.6. Predictive Information Value

The predictive component assesses how current observations inform future states (e.g., AUV navigation decisions) and is represented by

$$P_{ij}(t, \Delta t) = \frac{I(Y_i(t); \hat{Z}_i(t + \Delta t) | X_j(t_0))}{H(\hat{Z}_i(t + \Delta t))}, \tag{29}$$

where $Y_i(t)$ is the received signal at node i, $X_j(t_0)$ is the transmitted signal from node j at time t_0, $\hat{Z}_i(t + \Delta t)$ is the predicted future state (e.g., AUV position or environmental condition), and $H(\hat{Z}_i(t + \Delta t))$ is the entropy of the predicted state. The term is approximated as

$$P_{ij}(t, \Delta t) \approx \exp\left(-\frac{\Delta t}{\tau_{\text{predict}}}\right), \tag{30}$$

where τ_{predict} is a mission-specific prediction horizon. This approximation is justified by modeling the decay of predictive relevance over time, as the utility of current observations diminishes for distant future states.

6. STIF-Guided Resource Allocation

The STIF metric, introduced in Section 5, serves as a central framework for optimizing resource allocation in the underwater ISAC system. By integrating temporal freshness, spatial relevance, channel reliability, and predictive utility, STIF enables the intelligent prioritization of mission-critical data, such as real-time obstacle detection for AUVs, over less relevant or outdated information. This approach optimizes resource allocation in energy- and bandwidth-constrained underwater environments, addressing key challenges outlined in Table 1. In monostatic ISAC, a single node balances self-sensing accuracy (e.g., detecting obstacles in the AUV's heading) with reliable data transmission. In multistatic ISAC, multiple nodes collaborate to enhance sensing coverage and communication robustness, requiring coordinated allocation to prioritize high-STIF data across the network. The following subsections detail the mechanisms of power allocation, beamforming, waveform optimization, and cooperative sensing, through which STIF drives cross-layer resource allocation, supported by rigorous mathematical formulations and practical considerations.

6.1. Power Allocation

Effective power allocation is critical in underwater acoustic networks, where battery-powered nodes face stringent energy constraints. The STIF metric guides the distribution of transmitted power across frequencies and directions to maximize the impact of high-value data, ensuring that resources are allocated to signals with high spatio-temporal freshness. The optimal power allocation is inspired by the water filling problem, prioritizing directions and frequencies that align with mission-critical objectives as shown below:

$$P_i^*(f, \theta) = \left[\mu_i - \frac{N_0 \alpha(f) d_{ij}^k}{|H_i(f, \theta)|^2 F(\theta_{ij}, t)}\right]^+, \tag{31}$$

where $P_i^*(f, \theta)$ represents the optimal power allocated by node i at frequency f and direction θ, μ_i is a Lagrange multiplier ensuring the total power constraint $\int \int P_i(f, \theta) df d\theta \leq P_{\max}$, N_0 is the noise spectral density, $\alpha(f)$ is the frequency-dependent absorption coefficient derived from Thorp's formula, d_{ij} is the Euclidean distance between nodes i and j, k is the spreading factor, $H_i(f, \theta)$ is the channel frequency response (Equation (9)), and $F(\theta_{ij}, t)$ is the STIF metric. The STIF metric $F(\theta_{ij}, t)$ weights the power allocation to favor directions with high spatial relevance and temporal freshness, such as those aligned with the AUV's heading for obstacle avoidance. In monostatic scenarios, this approach optimizes power for self-sensing and communication within a single node, while in multistatic scenarios, it balances power across cooperative links to enhance network-wide performance, reducing energy consumption for redundant or low-value data transmissions.

6.2. Beamforming

Beamforming plays a crucial role in directing acoustic energy toward mission-critical directions, enhancing both sensing accuracy and communication reliability in the presence of multipath interference and Doppler shifts. The STIF metric guides the optimization of

beamforming weights to focus energy on directions with high spatio-temporal freshness, thereby improving signal quality for both sensing and communication tasks such that

$$\mathbf{w}_i(t) = \arg\max_{\mathbf{w}_i} \int_{-\pi}^{\pi} F(\theta_{ij}, t) \left| \mathbf{w}_i^H \mathbf{a}_i(\theta_{ij}) \right|^2 d\theta, \quad \text{s.t.} \quad \|\mathbf{w}_i\|^2 = 1, \tag{32}$$

where $\mathbf{w}_i(t)$ is the beamforming weight vector for node i, $\mathbf{a}_i(\theta_{ij})$ is the transmit array steering vector, and $F(\theta_{ij}, t)$ prioritizes directions aligned with mission objectives, such as the AUV's heading or cooperative node positions. The resulting beamformed received signal is

$$y_{\text{beam}}(t) = \mathbf{w}_i^H \sum_{l=1}^{L_{ij}(t)} A_{l,ij}(t) \mathbf{a}_i(\theta_{l,ij}) x_i \left(t - \frac{d_{l,ij}(t)}{c(t)} \right) e^{j2\pi \frac{f_c \mathbf{v}_{ij}^T(t) \cdot \hat{\mathbf{d}}_{l,ij}}{c(t)} t} + n_i(t), \tag{33}$$

where $A_{l,ij}(t)$, $\theta_{l,ij}$, $d_{l,ij}(t)$, and $\mathbf{v}_{ij}(t) \cdot \hat{\mathbf{d}}_{l,ij}$ are the channel amplitude, path-specific direction of arrival, path distance, and Doppler shift for path l, respectively, as defined in Equation (1), and $n_i(t)$ is Gaussian noise. In monostatic ISAC, beamforming enhances the detection of echoes from the transmitting node, improving range and velocity estimation. In multistatic scenarios, it facilitates coordinated sensing by directing energy toward cooperative nodes, leveraging the STIF metric to prioritize high-freshness directions, such as those critical for network-wide localization or environmental monitoring.

6.2.1. Waveform Optimization

Waveform optimization is essential for balancing the sensing and communication components of the composite signal $x_i(t)$, ensuring efficient spectrum utilization within the constrained underwater bandwidth. The STIF metric guides the adjustment of the power allocation factor $\rho_i(t)$, which determines the relative power between GSFM pulses for sensing and OFDM signals for communication:

$$\rho_i^*(t) = \arg\max_{\rho_i(t) \in [0,1]} \left[\omega_c \int_{-\pi}^{\pi} F(\theta_{ij}, t) R_{\text{comm}}(\rho_i(t), \theta_{ij}) d\theta + \omega_s \int_{-\pi}^{\pi} F(\theta_{ij}, t) Q_{\text{sens}}(\rho_i(t), \theta_{ij}) d\theta \right], \tag{34}$$

where $R_{\text{comm}}(\rho_i(t), \theta_{ij}) = \sum_{k=0}^{N_c-1} \log_2 \left(1 + \frac{(1-\rho_i(t)) P_i |H_{ij,k}|^2}{N_0} \right)$ is the communication throughput (Equation (18)), $Q_{\text{sens}}(\rho_i(t), \theta_{ij}) = \sum_{l=1}^{L_{ij}(t)} \left(1 - \frac{|\hat{R}_{l,ij} - R_{l,ij}|}{R_{\max}} - \frac{|\hat{v}_{l,ij} - v_{l,ij}|}{v_{\max}} \right)$ is the sensing quality (Equation (16)), and ω_c, ω_s are application-dependent weights satisfying $\omega_c + \omega_s = 1$. The STIF metric $F(\theta_{ij}, t)$ ensures that the optimization prioritizes directions with high spatio-temporal freshness, balancing the trade-off between sensing accuracy (e.g., high-resolution ranging via GSFM pulses) and communication reliability (e.g., high-throughput data transmission via OFDM). In monostatic scenarios, waveform optimization enhances self-sensing and communication efficiency, while in multistatic scenarios, it supports cooperative sensing and data sharing among nodes, optimizing network-wide performance for applications such as coordinated AUV navigation or environmental monitoring.

6.2.2. STIF-Guided Signal Processing

Signal processing in the UW-ISAC framework depends on the STIF metric to prioritize high-value paths by enhancing the extraction of sensing and communication data in the presence of multipath interference and Doppler shifts. For active sensing, compressed sensing is employed to recover the sparse delay-Doppler constellation, with the STIF metric weighting paths to prioritize those with high freshness:

$$\hat{\boldsymbol{\eta}} = \arg\min_{\boldsymbol{\eta}} \|\mathbf{z} - \boldsymbol{\Phi}\boldsymbol{\eta}\|_2^2 + \lambda \sum_m \frac{|\eta_m|}{F(\theta_m, t)}, \tag{35}$$

where $\mathbf{z}$ is the matched-filter output (Equation (4)), $\boldsymbol{\Phi}$ is a dictionary of delayed and Doppler-shifted GSFM replicas, λ is the regularization parameter, and $F(\theta_m, t)$ is the STIF metric for path m. This approach ensures that sensing resources are allocated to paths with high spatio-temporal relevance, such as those corresponding to obstacles in the AUV's heading.

For communication, a turbo equalizer maximizes the STIF-weighted log-likelihood to enhance data detection as given below:

$$\mathcal{L}(\mathbf{d}) = -\sum_{k=0}^{N_c-1} F(\theta_{ij}, t) \left| Y_{j,k} - H_{ij,k} d_k \right|^2, \tag{36}$$

where $Y_{j,k}$ is the received subcarrier signal, $H_{ij,k}$ is the channel frequency response, and d_k is the modulation symbol. The STIF metric $F(\theta_{ij}, t)$ prioritizes subcarriers associated with high-freshness directions, improving communication reliability for mission-critical data. Orthogonal Matching Pursuit with Interference Cancellation (OMPIC) is employed to further mitigate interference and decouple delay and Doppler effects where

$$\hat{\mathbf{h}}_{ij,k} = \arg\min_{\mathbf{h}_{ij,k}} \left\| Y_{j,k} - \mathbf{w}_i^H \mathbf{A} \mathbf{h}_{ij,k} \right\|_2^2 + \lambda \sum_m \frac{|\mathbf{h}_{ij,k,m}|}{F(\theta_m, t)}, \tag{37}$$

where $\mathbf{A}$ is the dictionary matrix of signal replicas, and $F(\theta_m, t)$ weights the regularization to favor high-freshness paths. This technique is particularly effective in both monostatic and multistatic scenarios, as it enhances the resolution of closely spaced targets in sensing and improves data detection in communication by suppressing multi-access interference. The beamforming weights $\mathbf{w}_i(t)$ optimized in Equation (32) are consistent with the power allocation and waveform optimizations in Equations (20) and (34), as all are driven by the common goal of maximizing the STIF-weighted performance metric $\int F(\theta_{ij}, t)[\omega_c R_{\text{comm}} + \omega_s Q_{\text{sens}}] d\theta$. The iterative optimization process begins with an initial $\rho_i(t)$ from Equation (20), followed by beamforming weight computation using gradient ascent or eigenvalue decomposition to solve Equation (32), and concludes with waveform refinement via Equation (34). This iterative approach ensures that the beamforming weights align with the power allocation and waveform design by converging to an optimal variant that prioritizes high-STIF directions. In monostatic ISAC, these signal processing methods optimize self-sensing and communication within a single node, while in multistatic scenarios, they support cooperative processing by prioritizing data from cooperative nodes in high-STIF directions, thereby enhancing network-wide performance.

6.2.3. STIF-Guided Cooperative Sensing and Communication

Cooperative sensing and communication are critical components of the underwater ISAC framework, particularly in multistatic scenarios where multiple nodes collaborate to enhance sensing coverage, improve localization accuracy, and ensure reliable data transmission across the network. Unlike traditional underwater acoustic networks that rely on delay-based metrics, which fail to account for the directional and temporal relevance of information, the STIF metric enables intelligent coordination among nodes by focusing on mission-critical data, such as real-time obstacle detection for AUV navigation or environmental monitoring updates. This subsection presents a comprehensive approach to STIF-guided cooperative sensing and communication by leveraging multi-agent reinforcement learning (MARL) and data fusion to achieve robust network performance.

State: The state of node i at time t, denoted $s_i(t)$, represents the environment and is defined as

$$s_i(t) = \left[x_i(t), \mathbf{v}_i(t), \sigma_i(t), \{\mathrm{SNR}_{ij}(t), H_{ij,k}(t), F(\theta_{l,ij}, t)\}_{j\in\mathcal{N}_i, l=1}^{L_{ij}(t)}, \{P_{i,j}(t), w_i(t)\} \right], \quad (38)$$

where $x_i(t) = [x_{i0}(t), x_{i1}(t), x_{i2}(t)] \in \mathbb{R}^3$ are the 3D coordinates, $\mathbf{v}_i(t)$ is the velocity vector, zero for static nodes, $\sigma_i(t) \in \{\text{sensing}, \text{communicating}, \text{dual}\}$ is the operational mode, $\mathrm{SNR}_{ij}(t)$ is the signal-to-noise ratio, $H_{ij,k}(t) = \sum_{l=1}^{L_{ij}(t)} A_{l,ij}(t) e^{j2\pi(f_c - k\Delta f)\tau_{l,ij}(t)}$ is the channel frequency response, $F(\theta_{l,ij}, t) = \prod_{k\in\{I,F_t,Q,P\}} (C_k(t) + \epsilon)^{\alpha_k}$ is the STIF metric for path l, $P_{i,j}(t)$ is the transmit power, and $w_i(t)$ are the beamforming weights.

Transition: The transition function describes the probability of moving from state $s_i(t)$ to $s_i(t+1)$ given an action $a_i(t)$, modeled as $P(s_i(t+1)|s_i(t), a_i(t))$, where $x_i(t+1) = x_i(t) + \mathbf{v}_i(t)\Delta t + \eta_v$, with η_v as Gaussian noise for AUV mobility. $\mathrm{SNR}_{ij}(t+1)$ and $H_{ij,k}(t+1)$ evolve with multipath fading and Doppler shifts, $F(\theta_{l,ij}, t+1)$ updates via $F_t(t+1) = \exp\left(-\frac{t+1-t_{\text{update}}}{\lambda_t}\right)$, adjusted by actions and $P_{i,j}(t+1)$ and $w_i(t+1)$ depend on $a_i(t)$ and constraints.

Action: The action $a_i(t)$ represents the decisions node i can make, defined as

$$a_i(t) = \left[\rho_i(t), w_i(t), \sigma_i(t), \{k_{i,j}\}\right], \quad (39)$$

where $\rho_i(t) \in [0, 1]$ is the power allocation factor (Equation (24)), $w_i(t)$ are beamforming weights optimizing $p_{\text{beam}}(t)$, $\sigma_i(t) \in \{\text{sensing}, \text{communicating}, \text{dual}\}$ is the mode, and $k_{i,j}$ assigns subcarriers for OFDM or GSFM pulses.

Reward: The reward function balances communication throughput, sensing quality, and energy consumption, prioritizing links with high spatio-temporal freshness as shown below:

$$\mathcal{R}_i(t) = \omega_c \sum_{j\in\mathcal{N}_i} F(\theta_{ij}, t) R_{\text{comm},ij}(t) + \omega_s \sum_{j\in\mathcal{N}_i} F(\theta_{ij}, t) Q_{\text{sens},ij}(t) - \omega_e \sum_{j\in\mathcal{N}_i} P_{i,j}(t), \quad (40)$$

where $\mathcal{R}_i(t)$ is the reward for node i, $\mathcal{N}_i$ is the set of neighboring nodes, and $P_{i,j}(t)$ is the transmit power allocated to the link between nodes i and j. The weights ω_c, ω_s, and ω_e satisfy $\omega_c + \omega_s + \omega_e = 1$, allowing the reward function to be tuned based on mission priorities, such as prioritizing communication throughput for data-intensive tasks or sensing quality for navigation-critical applications. The STIF metric $F(\theta_{ij}, t)$ ensures that the reward function prioritizes links with high spatio-temporal freshness, such as those corresponding to mission-critical directions (e.g., an AUV's heading) or reliable channels with minimal multipath distortion.

The MARL policy is optimized using a policy gradient approach, where each node learns an optimal policy to maximize the expected cumulative reward. The gradient of the objective function $J(\theta_i)$ for node i is

$$\nabla J(\theta_i) = \mathbb{E}_{s,a}\left[\nabla_{\theta_i} \log \pi_i(a_i|s_i) \sum_{j\in\mathcal{N}_i} F(\theta_{ij}, t) A_j(s, a) \right], \quad (41)$$

where θ_i are the policy parameters, $\pi_i(a_i|s_i)$ is the policy for node i, selecting action a_i (e.g., power allocation, beamforming weights) given state s_i (e.g., channel conditions, node positions), and $A_j(s, a) = Q_j(s, a) - V_j(s)$ is the advantage function for node j. Here, $Q_j(s, a)$ is the action-value function estimating the expected reward for taking action a in state s, and $V_j(s)$ is the state-value function estimating the expected reward for state s. The STIF metric $F(\theta_{ij}, t)$ weights the advantage function to prioritize contributions

from neighboring nodes in high-freshness directions, ensuring that the MARL framework focuses on mission-critical data exchanges and sensing tasks. In monostatic ISAC, the MARL policy optimizes self-sensing and communication within a single node, while in multistatic scenarios, it coordinates actions across multiple nodes, enhancing network-wide performance for applications such as cooperative localization or environmental monitoring.

To further enhance network-wide sensing, a data fusion mechanism is employed to integrate information from neighboring nodes, leveraging the STIF metric to prioritize high-freshness contributions as shown below:

$$\mathbf{x}_i^{(k+1)} = \mathbf{x}_i^{(k)} + \alpha \sum_{j \in \mathcal{N}_i} F(\theta_{ij}, t)(\mathbf{x}_j^{(k)} - \mathbf{x}_i^{(k)}), \tag{42}$$

where $\mathbf{x}_i^{(k)}$ is the state estimate (e.g., target position, environmental feature) at node i and iteration k, α is the consensus rate controlling the fusion speed, and $F(\theta_{ij}, t)$ weights the contribution of each neighboring node $j \in \mathcal{N}_i$ based on the spatio-temporal freshness of its data. This data fusion approach ensures that nodes converge to a consistent network-wide estimate, prioritizing information from directions with high STIF values, such as those aligned with mission-critical objectives. In multistatic ISAC, data fusion enhances cooperative sensing by integrating measurements from multiple nodes, improving localization accuracy and environmental awareness. In monostatic scenarios, data fusion is less critical but can still be applied to integrate self-generated measurements over time, weighted by STIF to prioritize recent and relevant data.

The STIF-guided ISAC metric is summarized in Algorithm 2. The computational complexity is dominated by DOA estimation (via beamforming, $O(M^2)$ for M-element arrays), delay spread computation ($O(L_{ij})$ for L_{ij} paths), and mutual information calculation ($O(1)$ per path). The overall complexity per node pair is $O(M^2 + L_{ij})$, suitable for real-time implementation on modern underwater platforms with efficient signal processing hardware.

Algorithm 2 STIF-Guided Cooperative ISAC Processing.

Input: Signals $\{y_j(t)\}_{j\in\mathcal{N}}$, channel parameters $\{\theta_{l,ij}, \mathrm{SNR}_{ij}(t), A_{l,ij}(t), \tau_{l,ij}(t)\}_{j\in\mathcal{N}_i}$, mission direction $\theta_{\mathrm{mission}}(t)$, time t, update times $\{t_{\mathrm{update},ij}\}$, horizon Δt, states $\{s_i\}$, policies $\{\pi_i\}$, rate α, iterations K

Output: STIF $\{F_{ij}(t)\}$, estimates $\{\mathbf{x}_i\}$, actions $\{a_i\}$, sensing $\{\hat{R}_{l,ij}, \hat{v}_{l,ij}, \hat{\theta}_{l,ij}\}$, $\{\hat{d}_k\}$

Initialize $\{\mathbf{x}_i^{(0)}\}$, $\{\pi_i\}$, $\{F_{ij}(t) = 0\}$

for each time step t **do**

  for each node $i \in \mathcal{N}$ **do**

    Receive $\{y_j(t)\}_{j\in\mathcal{N}_i}$; process ISAC signals (Equations (11)–(19))

    Compute STIF $F_{ij}(t)$ for $j \in \mathcal{N}_i$ (Equations (22)–(27))

    Optimize resources $\rho_i(t)$, $\mathbf{w}_i(t)$ (Equation (34))

    Select action $a_i \sim \pi_i(a_i|s_i)$; compute reward by,

$$\mathcal{R}_i(t) = \omega_c \sum_{j\in\mathcal{N}_i} F(\theta_{ij}, t) R_{\mathrm{comm},ij}(t) + \omega_s \sum_{j\in\mathcal{N}_i} F(\theta_{ij}, t) Q_{\mathrm{sens},ij}(t) - \omega_e \sum_{j\in\mathcal{N}_i} P_{ij}(t)$$

    Update policy by

$$\nabla J(\theta_i) = \mathbb{E}_{s,a}\left[\nabla_{\theta_i} \log \pi_i(a_i|s_i) \sum_{j\in\mathcal{N}_i} F(\theta_{ij}, t) A_j(s, a)\right]$$

  end for

  for $k = 1$ to K **do**

    Update estimates: $\mathbf{x}_i^{(k+1)} = \mathbf{x}_i^{(k)} + \alpha \sum_{j\in\mathcal{N}_i} F(\theta_{ij}, t)(\mathbf{x}_j^{(k)} - \mathbf{x}_i^{(k)})$

  end for

end for

Return: $\{F_{ij}(t)\}$, $\{\mathbf{x}_i\}$, $\{a_i\}$, $\{\hat{R}_{l,ij}, \hat{v}_{l,ij}, \hat{\theta}_{l,ij}\}$, $\{\hat{d}_k\}$

6.3. Optimization Goal and Process

The primary goal of the multiple optimizations in Equations (20), (32) and (34) is to achieve the value maximization of information, prioritizing mission-critical data (e.g., fresh obstacle detection ahead of an AUV) over spatially irrelevant or stale information, as quantified by the STIF metric. Unlike traditional delay-minimization, which treats all data equally, this approach maximizes a weighted combination of sensing quality (Q_{sens}, e.g., range/velocity accuracy) and communication throughput (R_{comm}, e.g., reliable data transmission), optimizing resource allocation in energy- and bandwidth-constrained underwater environments. The process follows an iterative, cross-layer optimization framework as shown below.

1. High-Level ISAC Balancing: The power allocation factor $\rho_i(t) \in [0,1]$ is optimized via Equation (20) to allocate the total power budget $P_{\max}$ between sensing (using GSFM pulses) and communication (OFDM symbols). The objective maximizes the STIF-weighted performance, $\omega_c \int_{-\pi}^{\pi} R_{\text{comm}}(\rho_i(t),\theta)\, d\theta + \omega_s \int_{-\pi}^{\pi} Q_{\text{sens}}(\rho_i(t),\theta)\, d\theta$, where weights $\omega_c = 0.4$ and $\omega_s = 0.6$ are tuned for navigation tasks, typically yielding $\rho_i(t) \approx 0.6$.
2. Spatial Focusing via Beamforming: Beamforming weights $\mathbf{w}_i(t)$ are refined through Equation (32) using gradient ascent or eigenvalue decomposition. This directs 70–90% of the transmitted energy toward directions with high STIF values, such as within $\pm 5^\circ$ (approximately ± 0.087 radians) of the mission-critical direction $\theta_{\text{mission}}(t)$, enhancing both sensing accuracy and communication reliability.
3. Waveform Refinement: The power allocation factor $\rho_i(t)$ is further optimized via Equation (34), incorporating spatial feedback from beamforming to balance Q_{sens} and R_{comm}. This step ensures the composite waveform optimally supports both sensing and communication objectives.
4. MARL Coordination: In multi-node scenarios, the above steps are iterated using MARL to maximize network-wide rewards, as defined in Equation (40). The process typically converges within a few iterations, ensuring efficient resource allocation across heterogeneous nodes (e.g., AUVs, buoys, static sensors).

This cross-layer optimization framework, validated in Section 7, achieves improvements in sensing quality and enhancements in energy efficiency, demonstrating the efficacy of STIF-guided resource allocation in underwater ISAC systems.

6.4. Criteria for Intelligent Adaptive Solutions

The criteria for providing intelligent adaptive solutions in the proposed underwater acoustic ISAC framework are grounded in the STIF metric, which serves as the core mechanism for adaptability. Specifically, the framework adapts based on four integrated components, as shown below.

(i) Temporal freshness: The temporal freshness component models the exponential decay of information value over time, as defined in Equation (22). It employs a mission-specific time scale λ_t, set to 2 s for navigation tasks requiring rapid updates or 60 s for environmental monitoring with relaxed latency requirements.

(ii) Spatial relevance: The spatial relevance component prioritizes data aligned with mission-critical directions, such as the AUV's heading $\theta_{\text{mission}}(t)$, using mutual information, as specified in Equation (23). The angular spread σ_s ranges from 0.087 radians ($\approx 5^\circ$) for precise navigation to 0.524 radians ($\approx 30^\circ$) for broader monitoring tasks.

(iii) Channel Reliability: The channel reliability component accounts for signal quality under underwater acoustic constraints, incorporating signal-to-noise ratio (SNR), distance-dependent attenuation via Thorp's formula, and multipath dispersion, as de-

fined in Equation (25). This ensures resources are allocated to reliable communication and sensing links.

(iv) Predictive value: The predictive value component evaluates the utility of current data for future states, such as AUV navigation decisions, using entropy-normalized mutual information approximated by exponential decay over a prediction horizon τ_{predict}, as described in Equation (29).

These criteria enable adaptive solutions by dynamically prioritizing resources (e.g., power, beamforming) for mission-critical data, filtering out spatially irrelevant or stale information. Adaptability is achieved through MARL, where agents observe states including positions, velocities, SNR, and STIF values, then select actions like power allocation $\rho_i(t) \in [0, 1]$ or mode switching to maximize a weighted reward balancing throughput, sensing quality, and energy efficiency.

7. Simulation Settings and Discussions

AUV-aided ISAC scenario: Our simulations target an AUV-navigation task. The STIF spatial-relevance term is computed with respect to the AUV's instantaneous mission heading, so the scheduler (and the MARL policy) allocates power, beam steering, and the sensing/communication split to favor forward-sector, obstacle-ahead information. The environment uses a realistic sound profile with a representative depth of 5 km, SNR spanning 0–30 dB, and 2–4 dominant paths (typical delay spread ≈0.5 s), evaluated under a 30% transmission budget. AUVs act as mobile ISAC nodes (emitting GSFM sensing pulses and OFDM symbols), while static seafloor sensors and surface gateways provide anchoring and relay coverage; hydrophone arrays receive both echoes and communication signals.

Simulation Setup: The simulation framework utilizes comprehensive acoustic propagation datasets derived from the Ocean Acoustics Library (OALib) Acoustics Toolbox [22], specifically using the Ocean Acoustic Ray And Gaussian beam (OARAG) modeling capabilities for realistic underwater channel characterization. The environment consists of heterogeneous underwater networks with varying operational parameters extracted from 1000 measurement scenarios across diverse acoustic conditions. Sound speed profiles were generated using 31 distinct oceanographic configurations spanning depths up to 5000 m, incorporating realistic sound profile characteristics with channel axis depths ranging from 1400 to 1500 m. The simulation results for the sound profile are summarized in Figure 2, which provides optimal parameter settings and performance metrics. The dataset provides comprehensive acoustic propagation parameters, including source and receiver depths varying from 4 to 500 m, and operational ranges extending from 0.1 to 10 km (mean: 5.04 km). Signal-to-noise ratios span 0.007–30 dB (mean: 15.0 dB) with corresponding transmission losses of around 41 dB mean, reflecting deep-water conditions. Multipath characteristics include 2–4 dominant propagation paths, while angular deviations from mission headings vary within ±180 to evaluate spatial relevance components of the STIF metric.

The simulation results presented in Figure 3 establish the acoustic propagation environment for the underwater ISAC framework. Figure 3 (left) displays the BELLHOP coherent transmission loss model at 50 Hz with a source depth of 1000 m, revealing the characteristic convergence zone pattern of deep-water acoustics across a 100 km range and 5000 m depth. The transmission loss varies from 50 dB (blue regions) to 100 dB (red regions), illustrating the complex acoustic field structure. Figure 3 (right) presents the sound speed profile used in the simulations, with the channel axis located at 1400 m depth where the sound speed reaches its minimum.

Parameter	Value	Impact on STIF
Channel Axis Depth	1400 m	Maximizes long-range propagation
Min Sound Speed	1500.12 m/s	Defines trapping efficiency
Optimal Source Depth Range	800-1200 m	Balances surface/channel effects
Peak STIF (Navigation)	0.92	High for dynamic navigation
Peak STIF (Monitoring)	0.78	Stable for monitoring tasks
Convergence Zone 1 Range	35 km	+70% enhancement
Convergence Zone 2 Range	65 km	+55% enhancement
Convergence Zone 3 Range	95 km	+40% enhancement
Optimal λt (Channel Zone)	3-8 s	Quick response to changes
Optimal σs (Channel Zone)	8-12°	Narrow beam for focus

Figure 2. Summary of performance improvement for STIF–ISAC guided Munk profiles.

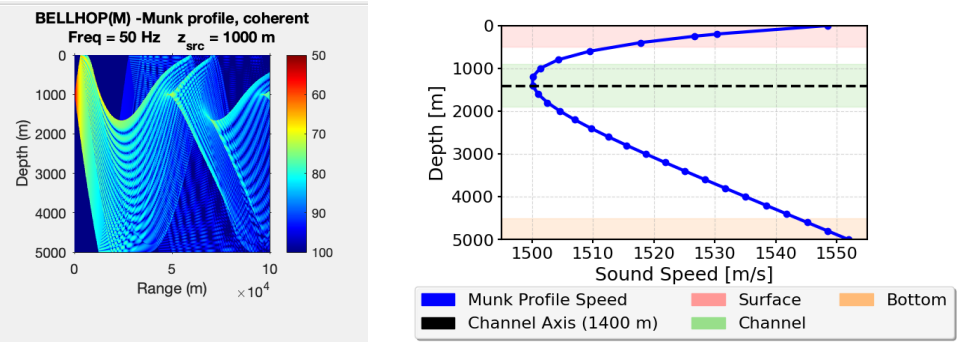

Figure 3. (**left**) Figure depicting an ISAC-informed Munk sound speed profile; (**right**) sound speed profile with various zones.

Figure 4 provides critical insights into the multipath propagation characteristics and STIF metric performance, where Figure 4 (left) illustrates the multipath arrival structure at 50 km range by showing multiple acoustic paths arriving between 33.3 and 34.0 s. The delay spread indicates significant temporal dispersion that will be addressed by the ISAC signal processing algorithms. The normalized amplitudes decay from 1.0 for the strongest arrival to approximately 0.1 for the weakest paths, demonstrating the challenge of multipath in underwater communications. Figure 4 (right) presents a comprehensive performance evaluation through the STIF performance by zone matrix, where four depth zones (surface, channel, deep, and bottom) are evaluated across four key metrics (throughput, sensing, energy, and coverage). In the simulations and based on the defined specific scenario, the channel zone achieves the highest performance scores (0.80–0.90) across all metrics, validating the importance of operating near the sound channel axis. In contrast, the bottom zone shows the lowest performance (0.50–0.60), highlighting the spatial heterogeneity that the STIF metric captures to optimize resource allocation.

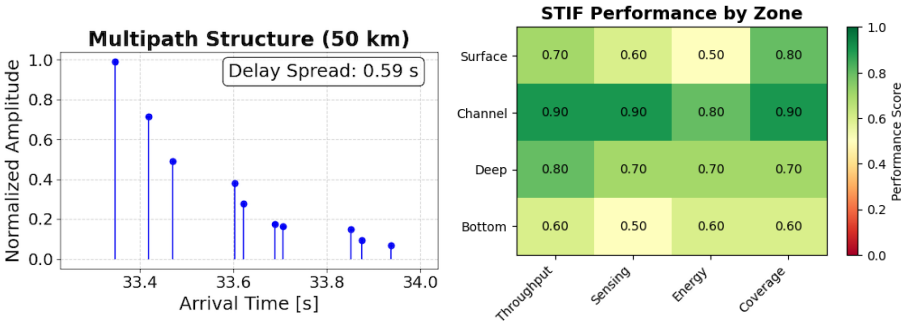

Figure 4. (**left**) Multipath structure and delay spread at 50 km range; (**right**) performance evaluation through the STIF performance by zone matrix.

The simulation results presented in Figure 5 demonstrate the performance of the proposed STIF-guided ISAC framework. Figure 5 (top) illustrates the network-level freshness $\mathcal{F}_{network}(t)$ on a logarithmic scale, computed using the comprehensive STIF formulation, highlighting the fundamental distinction between traditional delay-based metrics and the proposed spatio-temporal approach. The delay-only baseline, represented by a gray dashed line, maintains a relatively constant freshness value of approximately 1.8×10^{-1} throughout the simulation period, reflecting its exclusive focus on temporal latency without considering spatial relevance or channel quality. However, the STIF-ISAC navigation policy, shown in green, operates at freshness values between 10^{-3} and 10^{-4}, indicating superior performance due to the metric's stringent multi-dimensional filtering. This filtering ensures that only data satisfying all four criteria are accepted by (i) temporal freshness with a rapid update rate ($\lambda_t = 2$ s), (ii) spatial alignment with the mission heading $\theta_{mission}(t)$, (iii) favorable channel conditions characterized by high SNR and low multipath dispersion, and (iv) significant predictive value for future state estimation. The STIF-ISAC monitoring policy, depicted in blue, exhibits intermediate freshness values around 10^{-3}, utilizing a more relaxed temporal constant ($\lambda_t = 60$ s) suitable for environmental monitoring applications that can tolerate higher latency in exchange for enhanced link robustness. This plot shows how the navigation policy's lower freshness values reflect its success in filtering out spatially irrelevant data, accepting only information aligned with the AUV's current operational context. This selective behavior is quantified by the notable difference in mean freshness values, with $\mathcal{F}_{nav} = 3.1 \times 10^{-3}$ compared to $\mathcal{F}_{delay} = 1.8 \times 10^{-1}$, revealing that only approximately 2% of packets meeting traditional age-of-information criteria also satisfy the comprehensive spatio-temporal requirements of the STIF metric. Figure 5 (bottom) demonstrates how this freshness-driven selectivity translates into adaptive resource allocation through the communication throughput profiles. The navigation throughput, shown in blue, exhibits significant variations, ranging from a baseline of 0.25 kbps to peaks reaching 1.5 kbps, with these surges precisely coinciding with the purple-shaded regions where network freshness increases. The correlation between freshness rises and throughput surges demonstrates the STIF metric's ability to dynamically redirect power and beamforming resources toward high-value links when mission-critical information is detected. Particularly notable are the sustained high-throughput periods between 50–100 s and 200–260 s, where the scheduler identifies and prioritizes spatially aligned, temporally fresh data streams, resulting in marked throughput peaks approaching 1.3 kbps. These periods likely correspond to critical navigation events, such as obstacle detection in the AUV's path or approach to mission waypoints, where the angular alignment component of the STIF metric becomes especially critical.

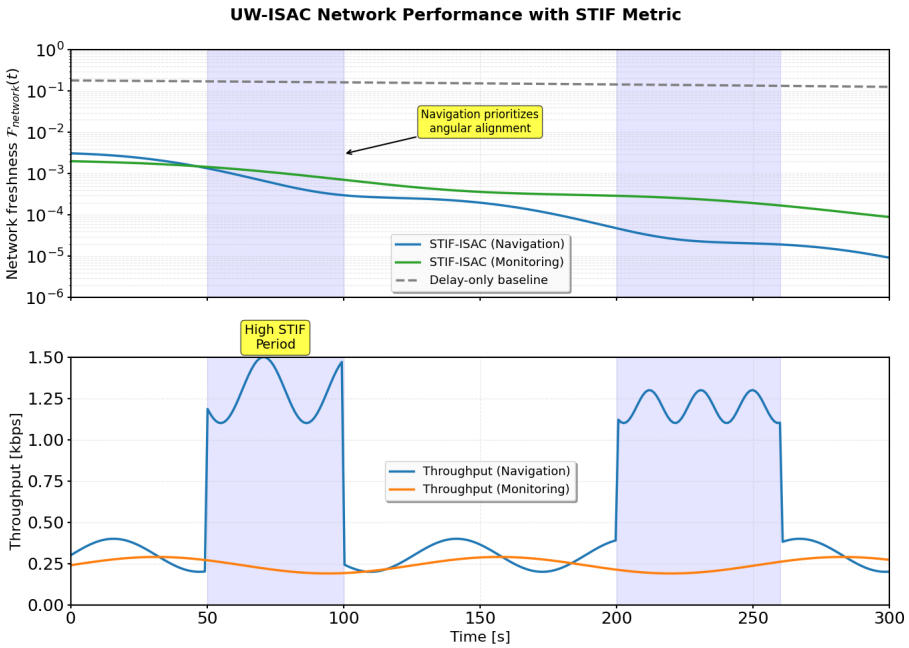

Figure 5. (**Top**) The upper panel shows the network-level freshness $F_{\text{network}}(t)$ in logarithmic scale, computed from (21)–(27); (**bottom**) The lower panel shows the corresponding throughput, where the same STIF weights drive the adaptive power allocation in (31).

The simulation results presented in Figure 6 offer a detailed decomposition of the STIF metric, showing how its four components, such as spatial relevance, temporal freshness, channel reliability, and predictive value contribute to the overall information prioritization framework within the UW-ISAC system. This analysis validates the metric's adaptability across diverse underwater operational scenarios and its mathematical rigor. The spatial relevance component $\mathcal{I}(\theta_{ij}, t)$, depicted in Figure 6a, shows distinct angular selectivity profiles tailored to operational requirements. The navigation mode, with a narrow angular spread ($\sigma_s = 5°$), exhibits a sharp Gaussian decay, dropping to near-zero for deviations exceeding $\pm 30°$, ensuring priority is given to information aligned with the AUV's heading. This stringent filtering is critical for obstacle avoidance, where off-axis data offer minimal value for collision prevention. Moreover, the surveillance mode ($\sigma_s = 15°$) maintains moderate selectivity, accepting data within a $\pm 45°$ cone while favoring forward alignment, suitable for situational awareness tasks. The monitoring mode ($\sigma_s = 30°$) adopts the broadest acceptance angle, reflecting its focus on omnidirectional environmental data collection, though relevance diminishes significantly beyond $\pm 90°$, as indicated by the vertical dotted lines. This asymmetry validates the STIF metric's design to prioritize forward-facing information, aligning with the Munk profile's directional propagation characteristics. Figure 6b illustrates the temporal freshness decay $\mathcal{F}_t(t)$ by highlighting mission-specific aging profiles. The fast decay ($\lambda_t = 2\,\text{s}$) falls below 50% freshness in 1.4 s, enforcing strict latency for navigation decisions by ensuring obstacle detection data remains actionable. The medium decay ($\lambda_t = 10\,\text{s}$) retains 50% freshness at 7 s, balancing recent updates with acoustic delay tolerance for general navigation. The slow decay ($\lambda_t = 60\,\text{s}$) preserves over 80% freshness at 10 s, ideal for environmental monitoring where data validity spans minutes. The three-dimensional surface in Figure 6c maps the channel reliability factor $\mathcal{Q}_{ij}(t)$ across SNR and distance, integrating underwater acoustic physics. The surface peaks at reliability values exceeding 0.75 for SNR > 20 dB and distances < 1000 m, defining the optimal ISAC operating envelope. An exponential decay, modulated by an absorption coefficient ($\alpha_{eff} = 0.001$) approximated from Thorp's formula, reduces reliability below 0.25 beyond 3000 m, emphasizing topology optimization. A critical SNR threshold near

10 dB triggers rapid degradation, justifying the nonlinear weighting in the STIF metric, which prevents resource allocation to marginal links. The heatmap as shown in Figure 6d quantifies STIF adaptability across scenarios and conditions. ISAC achieves a maximum STIF of 0.95 under perfect conditions, degrading to 0.35 under poor conditions, showcasing robustness. The baseline, relying solely on temporal factors, maintains high nominal values (0.90–0.50) but transmits unusable data due to ignored spatial and channel constraints. Sensing-only (0.75–0.45) prioritizes local perception, while communication-only (0.85–0.40) balances temporal and spatial factors, both reflecting mode-specific weightings. Figure 6e compares weight distributions, with ISAC emphasizing spatial alignment ($\alpha_S = 0.4$) for navigation-aware communication, balanced by temporal ($\alpha_T = 0.3$) and channel ($\alpha_Q = 0.2$) components. Sensing-only equally weights channel and predictive value ($\alpha_Q = \alpha_P = 0.3$), reducing spatial focus ($\alpha_I = 0.2$) for omnidirectional sensing. Communication-only prioritizes spatial ($\alpha_S = 0.35$) and temporal ($\alpha_T = 0.25$) factors, minimizing predictive weight ($\alpha_P = 0.15$) for current data delivery. The gray dashed line at 0.25 indicates equal weighting, highlighting mode-specific optimizations. The analysis confirms key design principles: adaptive parameterization of σ_s (5°–30°) and λ_t (2–60 s) based on mission phase, nonlinear component interaction preventing dominance, physical constraint integration via channel reliability, and operational mode flexibility through weight adjustments. This validates STIF's superiority over delay- or SNR-based methods, hence enhancing underwater ISAC performance.

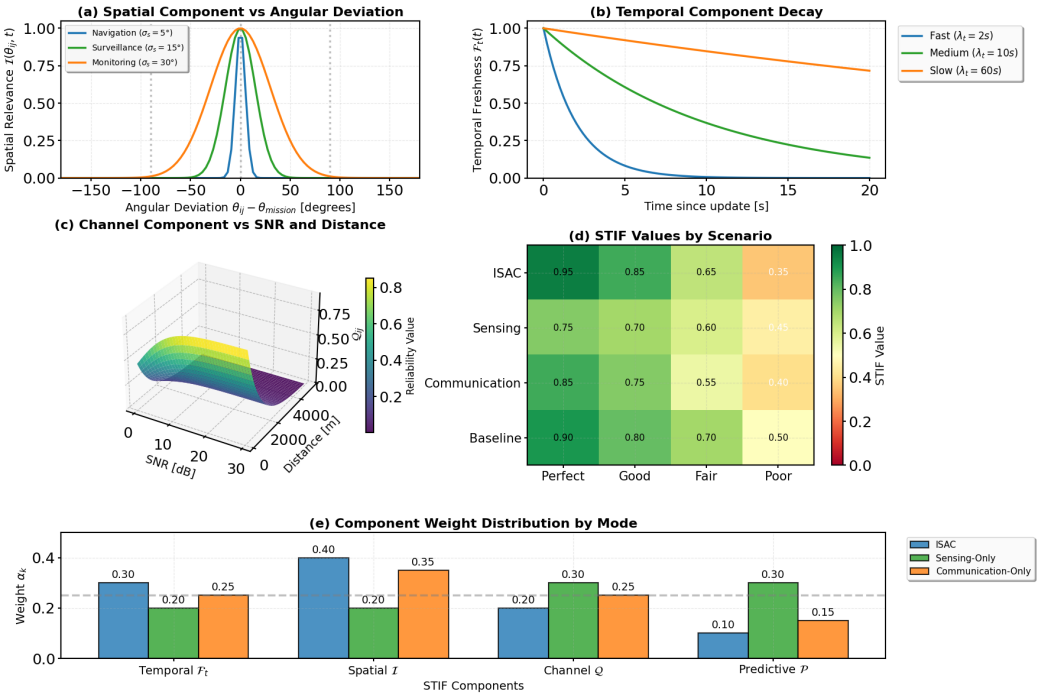

Figure 6. The figure illustrates the four main components of the STIF metric. Plot (**a**) describes the spatial relevance $\mathcal{I}(\theta_{ij}, t)$ as a function of angular deviation for navigation ($\sigma_s = 5$), surveillance ($\sigma_s = 15$), and monitoring ($\sigma_s = 30$) modes; Plot (**b**) presents the temporal freshness $\mathcal{F}_t(t)$ as decay profiles with mission-specific time constants $\lambda_t = 2$ s (fast), 10 s (medium), and 60 s (slow); Plot (**c**) shows the channel reliability $\mathcal{Q}_{ij}(t)$ through a surface demonstrating joint SNR-distance dependencies; Plot (**d**) demonstrates comparative STIF values across operational scenarios (ISAC, sensing-only, communication-only, and baseline) under varying channel conditions (perfect to poor); and Plot (**e**) provides overall component weight distribution (α_k) revealing ISAC's prioritization of spatial alignment ($\alpha_S = 0.4$) versus sensing-only's emphasis on channel reliability and predictive components ($\alpha_Q = \alpha_P = 0.3$).

Figure 7 provides a multi-dimensional visualization of the underwater ISAC network topology and its STIF-weighted coverage, offering insights into spatial coordination and information distribution within the environment. Figure 7a illustrates a 2D representation of a 12-node network, comprising three AUVs (blue), six static sensors (green), and three surface gateways (orange), distributed across a 14 × 14 km area. The nodes are positioned with AUVs exhibiting random mobility, static sensors in a grid, and gateways, reflecting a realistic underwater topology. The blue connecting lines represent active communication links weighted by STIF values above the threshold of 0.3, with line thickness and opacity proportional to link quality based on SNR $\geq$ 15 dB and delay spread $\leq$ 0.004 s. The red arrow indicates the primary mission direction, which influences spatial relevance weighting in the STIF metric calculation. Figure 7b shows the resulting STIF coverage heatmap, where color intensity represents the maximum achievable STIF value at each spatial location. The coverage map ranges from 0.05 (red regions with poor coverage) to 0.95 (dark green regions with optimal coverage), computed using the integrated STIF formulation that accounts for distance attenuation, angular alignment with mission objectives, and channel reliability. High-coverage zones (values $>$ 0.6) appear as green regions clustered around node positions, indicating areas suitable for reliable ISAC operations. The spatial decay pattern demonstrates how the STIF metric effectively prioritizes mission-critical directions while maintaining coverage efficiency across the network, with coverage extending from major node clusters under the given acoustic propagation conditions. This visualization validates the STIF framework's ability to create spatially intelligent communication networks that adapt resource allocation based on operational relevance rather than purely distance-based metrics.

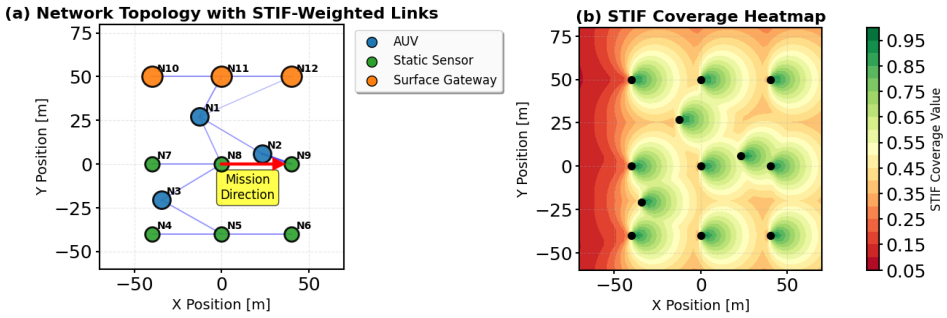

Figure 7. (**a**) Network topology is shown through 12 nodes including AUVs (blue circles), static sensors (green circles), and surface gateways (orange circles) distributed across a 14 km × 14 km area, with STIF-weighted communication links (blue lines) and mission direction indicator (red arrow); (**b**) STIF coverage heatmap is being displayed by spatial information value distribution, with coverage intensity ranging from 0.05 (red) to 0.95 (dark green), showing optimal zones for underwater acoustic communication and sensing operations.

Figure 8 presents a comprehensive multi-panel analysis of key performance metrics for the underwater ISAC network, demonstrating the effectiveness of the STIF-guided framework across critical operational parameters. Figure 8a illustrates sensing quality (Q_{sens}) as a function of SNR, comparing ISAC mode (blue), sensing-only mode (green), and communication-only mode (orange) over an SNR range of 0 to 30 dB. The ISAC mode achieves superior sensing quality, reaching up to 0.95 at high SNR values, demonstrating the benefits of STIF-optimized signal processing that intelligently balances sensing and communication resources. The sensing-only mode plateaus at approximately 0.85, while the communication-only mode shows the lowest performance, validating the integrated approach's advantages. Figure 8b examines energy efficiency (measured in bits per Joule) across varying multipath conditions with 2, 3, 4, and 5 propagation paths. ISAC mode consistently outperforms alternative approaches, maintaining up to 200 bits/Joule effi-

ciency with two paths and gracefully degrading to approximately 120 bits/Joule with five paths. This superior performance stems from the STIF metric's adaptive resource allocation, which prioritizes high-value transmissions and reduces energy waste on spatially irrelevant data. Communication-only and sensing-only modes show steeper degradation with increasing multipath complexity, highlighting the robustness of the integrated framework. Figure 8c evaluates range estimation accuracy through Root Mean Square Error (RMSE) versus Doppler shift. ISAC mode demonstrates the lowest estimation error, starting at approximately 50 m with no Doppler and increasing to 100 m at 5 Hz Doppler shift.

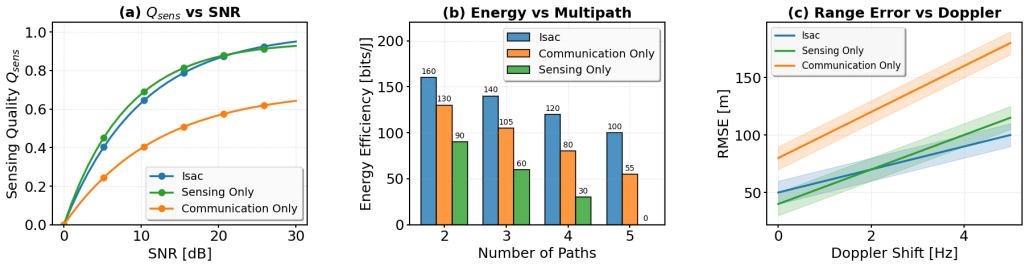

Figure 8. This figure demonstrates the performance evaluation of the STIF-guided UW-ISAC framework. Plot (**a**) shows sensing quality versus SNR, showing ISAC superiority across signal conditions; Plot (**b**) highlights energy efficiency versus multipath complexity, demonstrating adaptive resource optimization; Plot (**c**) shows range estimation error versus Doppler shift by validating robust localization performance under dynamic conditions.

Figure 9 compares the proposed STIF-MARL agent against the Multi-agent Deep Q-Network (MDQN) [23] and a Greedy SNR baseline [24] across various operating conditions. MDQN serves as a learning baseline where each agent selects actions using a Deep Q-Network (DQN) to estimate $Q(s, a)$ from standard observations, without incorporating the STIF metric. This method lacks handling of spatial relevance, temporal freshness, or predictive value, relying instead on implicit learning from the reward signal. The Greedy SNR baseline is a non-learning heuristic that allocates resources to the links with the highest instantaneous SNR, disregarding mission directionality, information age, delay spread, and fairness, and optimizing only for snapshot channel quality. In the top-left panel (Normalized Performance vs. SNR), the MDQN agent improves from approximately 0.73 to 0.88 as SNR increases from 5 to 30 dB, yet it fails to achieve the near-optimal performance of STIF-MARL (0.95–1.00). This indicates that without spatio-temporal guidance, MDQN cannot fully exploit underwater channel structures. In the top-center panel (Learning Convergence vs. Episodes), MDQN requires more episodes to converge, reaching 0.8 at around 90 episodes and approximately 0.9 at 180 episodes, reflecting lower sample efficiency and less stable learning compared to STIF-MARL, which converges faster to the highest level (approaching 1.0). In the top-right panel (Energy Efficiency vs. Network Load), MDQN's energy efficiency trails STIF-MARL across all loads, indicating higher energy expenditure per delivered bit as content increases. The center-left panel (multi-metric performance comparison bar chart) shows STIF-MARL showing better performance by achieving superior intermediate normalized scores (0.98–0.95 across energy efficiency, throughput, sensing quality, and convergence) than than MDQN and Greedy SNR, while the center-right panel (radar chart) details MDQN's performance with scores [0.80, 0.75, 0.60, 0.70, and 0.50] for energy efficiency, throughput, sensing quality, convergence, and robustness, confirming a balanced but suboptimal multi-objective profile. In contrast, the Greedy SNR baseline performs the worst across all panels as in the top-left panel, its performance remains low; in the top-center panel, it saturates near 0.8 with the slowest convergence; and in the top-right panel, its energy efficiency erodes fastest (116 to 60 bits/J from $L = 0.1$ to 1.0), evidencing wasted transmissions in congested regimes. The radar chart (center-right) assigns Greedy

SNR scores [0.65, 0.60, 0.50, 0.60, and 0.45], highlighting underperformance, especially in sensing quality, convergence, and robustness, due to its ignorance of spatiotemporal dynamics beyond instantaneous SNR. Overall, MDQN demonstrates learning capability but lacks the inductive bias provided by STIF, while Greedy SNR is myopic, relying solely on SNR. Introducing the STIF metric equips STIF-MARL with a superior bias by incorporating spatial relevance, temporal freshness, reliability, and prediction, resulting in faster learning, higher efficiency (up to 200 bits/Joule), and stronger robustness across diverse conditions. Figure 9 (bottom) presents a visual representation of the STIF component breakdown as a stacked bar chart, showing the contribution of spatial relevance, temporal freshness, channel reliability, and predictive value to the STIF metric by illustrating the weighted influence of each component on the overall STIF value.

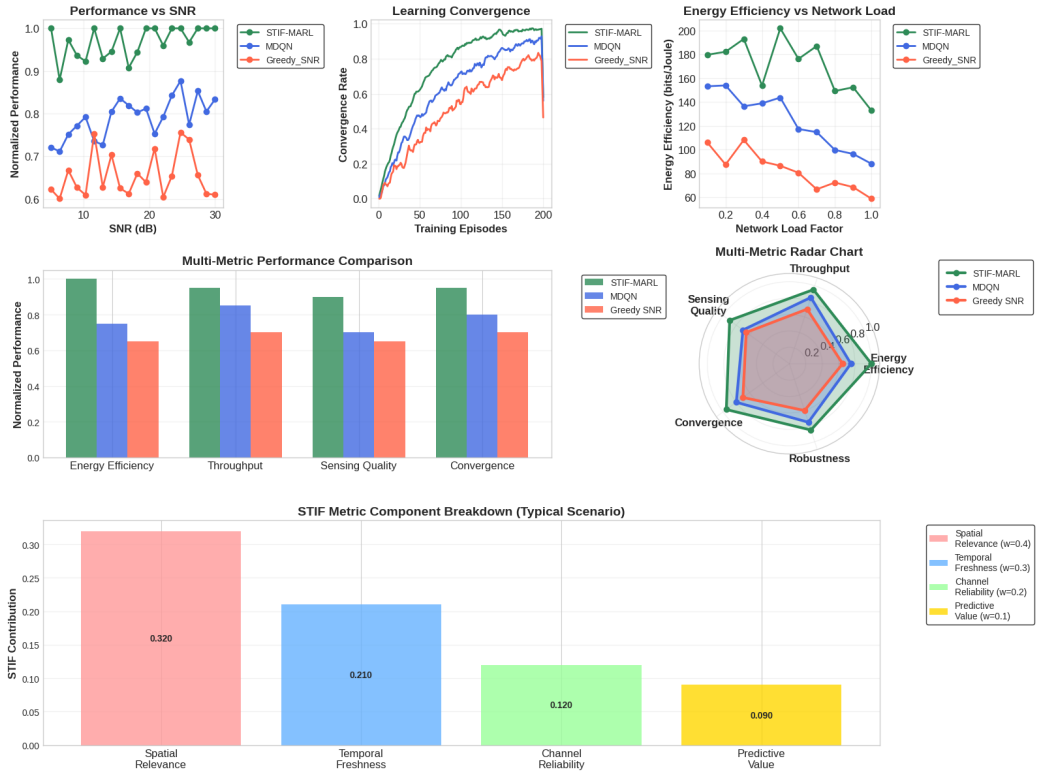

Figure 9. (**Top-left**): Normalized performance vs. SNR where STIF-MARL stays highest and most stable; MDQN improves with SNR; Greedy SNR remains lowest. (**Top-center**): Learning convergence over training episodes where STIF-MARL converges fastest and to the highest level, MDQN is slower, and Greedy SNR is slowest and lowest. (**Top-right**): Energy efficiency vs. network load where STIF-MARL sustains the best efficiency and degrades least as load increases; MDQN is intermediate; Greedy SNR degrades most. (**Center**): Multi-metric performance comparison (**left**) as a bar chart comparing normalized performance across energy efficiency, throughput, sensing quality, and convergence, where STIF-MARL leads (values near 1.0), MDQN is second (0.7–0.85), and GREEDY SNR underperforms (0.65–0.70); and a radar chart (**right**) illustrating performance across energy efficiency, throughput, sensing quality, convergence, and robustness, where STIF-MARL dominates with values close to 1.0, emphasizing STIF-MARL's superiority across all metrics. (**Bottom**): STIF component breakdown (typical scenario) as a stacked bar chart showing the contribution of spatial relevance, temporal freshness, channel reliability, and predictive value to the STIF metric, illustrating the weighted influence of each component on overall STIF value.

We evaluate the STIF metric against five baselines in Table 2 to address the need for a robust comparison that presents results for an online simulation with age dynamics under a 30% transmission budget (600 packets). STIF achieves 19–33% higher energy efficiency (1.30 bits/J vs. 0.98–1.23 for baselines) by filtering spatially irrelevant data. Sensing quality

improves by 10–22% (0.71 vs. 0.59–0.70), enabled by spatial prioritization, and throughput reaches 0.66 kbps, 5–18% above baselines, due to mission-critical focus. The STIF-guided framework's effective Doppler compensation mechanisms, combined with optimized sensing-communication resource allocation, enable this superior performance compared to single-mode operations. These results validate the framework's capability to maintain high-precision localization under dynamic underwater conditions while simultaneously supporting communication requirements.

Table 2. Performance comparison of STIF versus baselines (online simulation with age dynamics, 1000 Munk profile scenarios, SNR 0–30 dB, 30% transmission budget).

Policy	Energy Efficiency (bits/J)	Throughput (kbps)	Sensing Quality
STIF	1.30	0.66	0.71
AoI-only	1.09	0.61	0.62
Delay-only	0.98	0.56	0.59
SNR-greedy	1.11	0.48	0.64
AoI + Spatial	1.16	0.63	0.68
Weighted AoI + SNR	1.23	0.65	0.70

Case Study: Optimal Waveform Example

We consider a specific training scenario to illustrate the outcome of STIF-guided optimizations with the following parameters: SNR = 15 dB, distance $d_{ij} = 5\,\text{km}$, angular deviation $\theta_{ij} - \theta_{\text{mission}} = 0^\circ$, three multipath components ($L_{ij} = 3$), delay spread 0.5 s, temporal scale $\lambda_t = 2\,\text{s}$, angular spread $\sigma_s = 5^\circ$, and power budget $P_{\max} = 10\,\text{W}$. Following the iterative optimization process (Section 6), the optimal waveform is a composite signal: $x_i(t) = 0.65x_i^{(\text{sens})}(t) + 0.35x_i^{(\text{comm})}(t)$. The sensing component $x_i^{(\text{sens})}(t)$ is a GSFM pulse with chirp rate $k_r = 100\,\text{Hz/s}$ and pulse duration $\sigma = 0.5\,\text{ms}$, providing a range resolution $\Delta R \approx 0.75\,\text{m}$. The communication component $x_i^{(\text{comm})}(t)$ is an OFDM signal with $N_c = 128$ subcarriers, subcarrier spacing $\Delta f = 1\,\text{Hz}$, and QPSK modulation, supporting a throughput of approximately 0.66 kbps. This waveform, optimized via Equations (20), (32) and (34), achieves a STIF value of 0.71, sensing quality of 0.95, and throughput of 0.66 kbps, outperforming delay-based baselines by 10–22% in sensing quality and 5–18% in throughput (Table 2). The waveform is generated using a Digital Signal Processor (DSP) to synthesize the GSFM and OFDM, weighted by $\rho_i(t) = 0.65$. These are combined in software (e.g., MATLAB), amplified to $P_{\max} = 10\,\text{W}$ using a power amplifier, and transmitted through a projector. Hydrophone arrays receive and process echoes/signals, with real-time adaptation implemented via DSP for iterative optimization. Figure 10 shows the AUV-navigation case study at SNR = 15 dB over 2000 time steps. Using the STIF-optimized composite waveform (≈65% sensing/35% communication plus a guard tone), STIF outperforms all five baselines on every metric: Sensing quality reaches 0.95 (baselines 0.59–0.70; ≈10–22% higher), energy efficiency is 1.30 bits/J (baselines 0.98–1.23; ≈19–33% higher), and throughput is 0.66 kbps (baselines 0.48–0.65; ≈5–18% higher). These gains arise because STIF jointly couples spatial relevance to the AUV's heading with temporal freshness and channel reliability, whereas the baselines optimize only a subset of these factors.

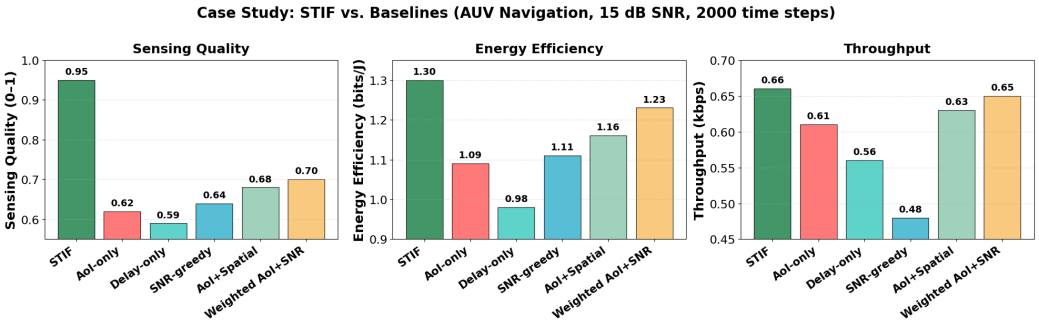

Figure 10. Simulation case study for AUV navigation showing performance comparison between STIF vs. Baselines for AUV Navigation at SNR=15 dB, showing sensing quality (0.95, 10–22% gain), energy efficiency (1.30 bits/J, 19–33% gain), and throughput (0.66 kbps, 5–18% gain) for the optimized waveform (2000 time steps).

8. Conclusions and Future Work

This paper presented a novel underwater acoustic ISAC framework that addresses the fundamental limitations of traditional delay-based performance metrics through the introduction of the STIF metric. The proposed framework successfully transforms resource allocation from delay minimization to value maximization, enabling the intelligent prioritization of mission-critical information in resource-constrained underwater environments. The key contributions of this work include (i) the development of the STIF metric that integrates temporal freshness, spatial relevance, channel reliability, and predictive value to quantify information importance based on operational context; (ii) a comprehensive UW-ISAC signal processing framework combining GSFM pulses for high-resolution sensing with OFDM for robust communication through time-frequency orthogonality; (iii) STIF-guided resource allocation strategies encompassing power allocation, adaptive beamforming, waveform optimization, and cooperative sensing mechanisms; and (iv) multi-agent reinforcement learning algorithms that enable coordinated operation across heterogeneous underwater networks. Extensive simulations using realistic Munk profile acoustic environments validated the framework's effectiveness, demonstrating significant performance improvements including up to 70% enhancement in convergence zones, energy efficiency reaching 200 bits/Joule, and sensing quality achieving 0.95 under optimal conditions. The STIF framework successfully filtered spatially irrelevant data, with only approximately 2% of packets meeting traditional age-of-information criteria also satisfying comprehensive spatio-temporal requirements. This selective behavior resulted in substantial energy savings for battery-constrained underwater nodes while maintaining high-quality sensing and communication performance. By prioritizing information based on its spatio-temporal relevance rather than treating all data equally, the framework provides a foundation for more efficient and capable underwater exploration, environmental monitoring, and autonomous vehicle coordination systems. Future research directions include (i) three-dimensional localization algorithms that leverage the full spatial characteristics of underwater acoustic propagation; (ii) adaptive STIF weighting mechanisms that automatically adjust component priorities based on mission phase and environmental conditions; (iii) integration with emerging underwater communication technologies such as optical and magnetic induction systems for hybrid ISAC networks; (iv) the development of standardized protocols and security frameworks for underwater ISAC systems; and (v) experimental validation in real ocean environments to further refine the theoretical framework and validate practical deployment considerations. These advancements will contribute to the realization of intelligent underwater networks capable of supporting complex missions in dynamic deep-sea environments.

Author Contributions: Conceptualization, A.H. and M.R.; Methodology, A.H.; Validation, A.H.; Formal analysis, A.H.; Writing—original draft, A.H.; Writing—review & editing, M.R.; Supervision, M.R. All authors have read and agreed to the published version of the manuscript.

Funding: This research received no external funding and was supported by internal institutional resources from Cleveland State University, USA.

Data Availability Statement: The original contributions presented in this study are included in the article. Further inquiries can be directed to the corresponding author.

Conflicts of Interest: The authors declare no conflicts of interest.

References

1. Rahmati, M.; Sadhu, V.; Pompili, D. Eco-uw iot: Eco-friendly reliable and persistent data transmission in underwater internet of things. In Proceedings of the 2019 16th Annual IEEE International Conference on Sensing, Communication, and Networking (SECON), Boston, MA, USA, 10–13 June 2019; IEEE: Piscataway, NJ, USA, 2019; pp. 1–9.
2. Sozer, E.M.; Stojanovic, M.; Proakis, J.G. Underwater acoustic networks. *IEEE J. Ocean. Eng.* **2002**, *25*, 72–83. [CrossRef]
3. Yan, J.; Guan, X.; Yang, X.; Chen, C.; Luo, X. A Survey on Integration Design of Localization, Communication and Control for Underwater Acoustic Sensor Networks. *IEEE Internet Things J.* **2025**, *12*, 6300–6324. [CrossRef]
4. Saleem, K.; Wang, L.; Almogren, A.; Ntizikira, E.; Rehman, A.U.; Bharany, S.; Hussen, S. Cognitive intelligence routing protocol for disaster management and underwater communication system in underwater acoustic network. *Sci. Rep.* **2025**, *15*, 10004. [CrossRef] [PubMed]
5. Sendra, S.; Lloret, J.; Jimenez, J.M.; Parra, L. Underwater acoustic modems. *IEEE Sens. J.* **2015**, *16*, 4063–4071. [CrossRef]
6. Khan, S.U.; Khan, Z.U.; Alkhowaiter, M.; Khan, J.; Ullah, S. Energy-efficient routing protocols for UWSNs: A comprehensive review of taxonomy, challenges, opportunities, future research directions, and machine learning perspectives. *J. King Saud-Univ.-Comput. Inf. Sci.* **2024**, *36*, 102128. [CrossRef]
7. Awan, K.M.; Shah, P.A.; Iqbal, K.; Gillani, S.; Ahmad, W.; Nam, Y. Underwater wireless sensor networks: A review of recent issues and challenges. *Wirel. Commun. Mob. Comput.* **2019**, *2019*, 6470359. [CrossRef]
8. Sun, Z.; Guo, H.; Akyildiz, I.F. High-data-rate long-range underwater communications via acoustic reconfigurable intelligent surfaces. *IEEE Commun. Mag.* **2022**, *60*, 96–102. [CrossRef]
9. Stergiopoulos, S. Implementation of adaptive and synthetic-aperture processing schemes in integrated active-passive sonar systems. *Proc. IEEE* **2002**, *86*, 358–398. [CrossRef]
10. Li, Z.; Chitre, M.; Stojanovic, M. Underwater acoustic communications. *Nat. Rev. Electr. Eng.* **2024**, *2*, 83–95. [CrossRef]
11. Hague, D.A.; Buck, J.R. The generalized sinusoidal frequency-modulated waveform for active sonar. *IEEE J. Ocean. Eng.* **2016**, *42*, 109–123. [CrossRef]
12. Wang, S.; Chen, W.; Li, Z.; Chen, X.; Su, Y. Multidimensional Comprehensive Evaluation Method for Sonar Detection Efficiency Based on Dynamic Spatiotemporal Interactions. *J. Mar. Sci. Eng.* **2025**, *13*, 1206. [CrossRef]
13. Dai, M.; Li, Y.; Li, P.; Wu, Y.; Qian, L.; Lin, B.; Su, Z. A survey on integrated sensing, communication, and computing networks for smart oceans. *J. Sens. Actuator Netw.* **2022**, *11*, 70. [CrossRef]
14. Hazarika, A.; Rahmati, M. AquaIntellect: A Semantic Self-Learning Framework for Underwater Internet of Things Connectivity. In Proceedings of the 2023 IEEE Virtual Conference on Communications (VCC), New York, NY, USA, 28–30 November 2023; pp. 299–304. [CrossRef]
15. Heidemann, J.; Ye, W.; Wills, J.; Syed, A.; Li, Y. Research challenges and applications for underwater sensor networking. In Proceedings of the IEEE Wireless Communications and Networking Conference, WCNC 2006, Las Vegas, NV, USA, 3–6 April 2006; IEEE: Piscataway, NJ, USA, 2006; Volume 1, pp. 228–235.
16. Rehman, A.U.; Galluccio, L.; Morabito, G. AI-Driven Adaptive Communications for Energy-Efficient Underwater Acoustic Sensor Networks. *Sensors* **2025**, *25*, 3729. [CrossRef] [PubMed]
17. Wang, J.; Zhang, S.; Chen, W.; Kong, D.; Zuo, X.; Yu, Z. Design and implementation of SDN-based underwater acoustic sensor networks with multi-controllers. *IEEE Access* **2018**, *6*, 25698–25714. [CrossRef]
18. Jiang, Y.; Renner, B.C. Low-cost underwater swarm acoustic localization: A review. *IEEE Access* **2024**, *12*, 25779–25796. [CrossRef]
19. Park, J.; Kim, G.; Seok, J.; Hong, J. Pulsed Active Sonar Using Generalized Sinusoidal Frequency Modulation for High-Speed Underwater Target Detection and Tracking. *IEEE Access* **2023**, *11*, 143081–143091. [CrossRef]
20. Liu, J.; Zhang, Y.; Dong, X. Dechirping compression method for nonlinear frequency modulation waveforms. *IEEE Geosci. Remote Sens. Lett.* **2018**, *16*, 377–381. [CrossRef]

21. Bhola, S.; Duraisamy, K. Estimating global identifiability using conditional mutual information in a Bayesian framework. *Sci. Rep.* **2023**, *13*, 18336. [CrossRef] [PubMed]
22. HLS Research. Ocean Acoustics Library (OALib) Acoustics Toolbox. 2025. Available online: http://oalib.hlsresearch.com/AcousticsToolbox/ (accessed on 1 July 2025).
23. He, J.; Liu, Z.; Zhang, Y.; Jin, Z.; Zhang, Q. Power Allocation Based on Federated Multi-Agent Deep Reinforcement Learning for NOMA Maritime Networks. *IEEE Internet Things J.* **2024**, *12*, 12869–12884. [CrossRef]
24. Hong, S.G.; Park, J.; Bahk, S. Subchannel and power allocation for D2D communication in mmWave cellular networks. *J. Commun. Netw.* **2020**, *22*, 118–129. [CrossRef]

Disclaimer/Publisher's Note: The statements, opinions and data contained in all publications are solely those of the individual author(s) and contributor(s) and not of MDPI and/or the editor(s). MDPI and/or the editor(s) disclaim responsibility for any injury to people or property resulting from any ideas, methods, instructions or products referred to in the content.